REPORT NO. DOT-TSC-OST-73-22

COMPARATIVE STUDIES OF THE SUPERSONIC JET NOISE GENERATED BY RECTANGULAR AND AXISYMMETRIC NOZZLES

Khoon Cheang Low, Jean F. Louis

JUNE 1973
FINAL REPORT

Prepared for:
DEPARTMENT OF TRANSPORTATION
OFFICE OF THE SECRETARY
Office of Noise Abatement
Washington DC 20590

The contents of this report reflect the views of the authors who are responsible for the facts and the accuracy of the data presented herein. The contents do not necessarily reflect the official views or policy of the Department of Transportation. This report does not constitute a standard, specification or regulation.

Technical Report Documentation Page

1. Report No.	2. Government Accession No.	3. Recipient's Catalog No.
DOT-TSC-OST-73-22		

4. Title and Subtitle	5. Report Date
COMPARATIVE STUDIES OF THE SUPERSONIC JET NOISE GENERATED BY RECTANGULAR AND AXISYMMETRIC NOZZLES	June 1973
	6. Performing Organization Code
7. Author(s)	8. Performing Organization Report No.
Khoon Cheang Low, Jean F. Louis*	None
9. Performing Organization Name and Address	10. Work Unit No. (TRAIS)
Department of Aeronautics and Astronautics Massachusetts Institute of Technology Cambridge, MA 02139	OS307/R3530
	11. Contract or Grant No.
	DOT-TSC-142
12. Sponsoring Agency Name and Address	13. Type of Report and Period Covered
Department of Transportation Office of the Secretary Office of Noise Abatement Washington DC 20590	Final Report Oct. 1971-Dec. 1972
	14. Sponsoring Agency Code

15. Supplementary Notes

*Under Contract to: Department of Transportation
Transportation Systems Center
Kendall Square
Cambridge, MA 02142

16. Abstract

The main purpose of this study is to develop experimental scaling laws useful for predicting the overall sound power of supersonic jets operating under a range of high stagnation temperatures and pressures and under various exit Mach numbers. A shock tube is used as a flexible tool to provide the range of high stagnation temperatures and pressures associated with the supersonic jets in this investigation. The range of stagnation pressures chosen (for a given temperature and Mach number) correspond to overexpanded, perfectly expanded and underexpanded conditions of the jet. Two different nozzle configurations: a rectangular and an axisymmetric, are examined to determine how a basic difference in shape of the jet changes the relative importance of the different noise generating mechanisms. Measured sound directivity and Mach waves propagation direction obtained from shadowgraphs indicate that Mach waves contribute importantly to the noise produced by a rectangular jet. Similar measurements made on the axisymmetric jet indicate stronger influence of shock-induced noise and in particular of shock turbulence interaction. To guide the formulation of scaling laws for the prediction of overall sound power, a theoretical model is proposed which derives expressions for the power sound level associated with Mach waves and for shock turbulence interaction. Concurrent use of the model and of experimental data allow the formulation of scaling laws for the overall sound power. The quasi two-dimensional flow from the rectangular nozzle gave an opportunity to study Mach and nozzle lip waves for both low and high temperature jets.

17. Key Words	18. Distribution Statement
Supersonic jet noise, Axisymmetric nozzle, Rectangular nozzle, Mach wave, Turbulence shock interaction, Scaling laws of supersonic jet noise	DOCUMENT IS AVAILABLE TO THE PUBLIC THROUGH THE NATIONAL TECHNICAL INFORMATION SERVICE, SPRINGFIELD, VIRGINIA 22151.

19. Security Classif. (of this report)	20. Security Classif. (of this page)	21. No. of Pages	22. Price
Unclassified	Unclassified	118	

Form DOT F 1700.7 (8-72) Reproduction of completed page authorized

PREFACE

The first phase of the work under Contract No. DOT-TSC-142 is described in Report No. DOT-TSC-142-1 (Louis, J. F. "A Systematic Study of Supersonic Jet Noise", December 1971) and in AIAA Paper No. 72-641 (Louis, J. F., Letty, R. P. and Patel, J. R., "A Systematic Study of Supersonic Jet Noise", 1972).

Recently, Messrs. Ara M. Demirjian and Vijay K. Singhal contributed to some of the measurements and analyses of supersonic jet noise.

This Final Technical Report was monitored by Mr. Raymond Ehrenbeck, DOT Transportation Systems Center.

TABLE OF CONTENTS

TABLE OF CONTENTS (continued)

LIST OF SYMBOLS

A_o	experimental constant
a	arbitrary parameter
$b_{i's}$	arbitrary variables
c	velocity of sound
C_a	ambient sound velocity
C_J	sound velocity at jet static temperature
D,d	diameter at exit plane of nozzle
dZ_{is}	transfer functions
$F(M_J)$	function of jet Mach numbers
$f_o(M_J)$	function of jet Mach numbers
$g_o(M_J)$	function of jet Mach numbers
I	acoustic intensity
g_i^2	statistical representation of the mean square value of input disturbance fields
K_1	experimental constant
K,k	wave numbers
L_s	length of supersonic region of perfectly expanded jet
L_s^*	supersonic length
ℓ	turbulent correlation radius
m	ratio of U_n over U_n^1
M_c	mean convective Mach number
M_s	shock Mach number
M_J	jet exit Mach number
n	number of shock cells in supersonic length
OPWL	overall sound power level

LIST OF SYMBOLS (continued)

P_J	jet static pressure
P_o	stagnation or total pressure
$P_{o\ perf}$	stagnation pressure required to produce perfectly expanded flow at the nozzle exit ($P_J = P_a$)
PWL	total sound power level
p_{ij}	compressive stress tensor
$\overline{(\frac{p}{p})^2}$	mean square value of the pressure fluctuations
p	pressure
p^*	local static pressure
RMS	root mean square
R^*	pressure ratio
R_c^*	critical pressure ratio
Re_{D_J}	Reynolds number based on the viscosity of the test gas (argon)
Re_{D_a}	Reynolds number based on the viscosity of the ambient air
s	shock separation, entropy
S	shock wave
SPL	sound pressure level
S_p^v	average values of transfer functions
T_J	jet static temperature
T_o	total or stagnation temperature
$T_{o\ perf}$	total temperature which gives static temperature as the ambient temperature
$\overline{T^2}$	typical mean square value of the strength of the sources

LIST OF SYMBOLS (continued)

T_{ij}	applied fluctuating stresses
T_p^v	transfer functions
U_J	jet velocity
U_n	component of mean flow velocity normal to shock wave
U_1, U_2, U_3	perturbing velocities in the 3 directions
$\underline{U}$	velocity vector
$\bigcup$	mean flow velocity
$\overline{U_w}$ $\overline{U_n}$	mean square value of the vorticity fluctuation
V	propagation velocity of disturbance
W_e	acoustic output per unit exit diameter
$\overline{W_e}$	total acoustic power from the supersonic region
V_e	volume of a typical eddy
α	experimental constant
β	experimental constant
θ	direction in which the Mach waves are propagating
μ_J	viscosity of argon gas
μ_a	viscosity of the ambient air
ρ_a	ambient air density
ρ_I	typical eddy density
ρ_J	jet density
$\rho v_i v_j$	fluctuating Reynolds stresses
σ	angle in which discontinuity is disturbed due to the upstream disturbance

LIST OF SYMBOLS (continued)

ϕ_1	arbitrary constant for density of eddy
ϕ_2	arbitrary parameter for RMS turbulent velocity
$\Phi_{ij}(k)$	spectral tensor
Ω	vorticity
ω	typical radian frequency of fluctuation
$\mathfrak{D}(M)$	turning angle through a Prandtl-Meyer expansion fan

---

Subscripts

J or j	jet static condition
a	ambient condition
o or 5	stagnation
1	1st shock
2	2nd shock

Prime	properties downstream of shock
*	local properties

ABSTRACT

The main purpose of this study is to develop experimental scaling laws useful for predicting the overall sound power of supersonic jets operating under a range of high stagnation temperatures and pressures and under various exit Mach numbers. A shock tube is used as a flexible tool to provide the range of high stagnation temperatures and pressures associated with the supersonic jets in this investigation. The range of stagnation pressures chosen (for a given temperature and Mach number) correspond to overexpanded, perfectly expanded and underexpanded conditions of the jet. Two different nozzle configurations: a rectangular and an axisymmetric, are examined in the study to determine how a basic difference in shape of the jet changes the relative importance of the different noise generating mechanisms. Indeed, the results indicate that the acoustic powers from a rectangular and an axisymmetric jet operated under identical flow parameters show different dependence on the scaling parameters, thus establishing the importance of different noise mechanisms on different nozzle configurations.

Because of the two-dimensionality of the rectangular jet, the system of the shocks through which the flow decelerates is very much shorter than in the identical axisymmetric jet. Noise mechanisms induced at the surface of the jet are therefore found to be dominant in the rectangular jet, whereas volume phenomena such as shock-induced noise are more important in the axisymmetric jet.

Measured sound directivity and Mach waves propagation direction obtained from shadowgraphs indicate that Mach waves contribute importantly to the noise produced by a rectangular jet. Similar measurements made on the axisymmetric jet indicate stronger influence of shock induced noise and in particular of shock turbulence interaction.

In order to guide the formulation of scaling laws for the prediction of overall sound power, a theoretical model is proposed. The model derives expressions for the power sound level associated with Mach waves and for shock turbulence interaction. The concurrent use of the model and of the experimental data allow the formulation of scaling laws for the overall sound power.

The quasi two-dimensional flow from the rectangular nozzle gave an opportunity to study Mach and nozzle lip waves for both low and high temperature jets. Statistical observations made on an ensemble of runs indicate that lip waves have well-defined frequency peaks and that these waves are out of phase when detected by two microphones located symmetrically relative to the jet. Similar Mach waves measurements indicate that these waves do not appear to have a constant phase relationship. At low temperature, with jet density nearly equal to ambient air density, lip waves frequencies are also found in the Mach waves spectrum, therefore indicating that lip disturbances propagate and grow along the shear layer. At high temperature, with jet density much smaller than ambient air density, the Mach waves spectrum is found to have no relation to the lip waves spectrum, and shear layer instabilities dominate the Mach waves field.

I. INTRODUCTION

The problem of jet noise reduction is a very difficult problem basically because the acoustic energy radiated is only a fraction of one percent of the jet kinetic energy and a considerable reduction in jet kinetic energy has to be made before there can be any appreciable reduction in the acoustic energy; in doing so the propulsive thrust and efficiency are reduced accordingly. Hence, any proposed scheme of noise reduction would have to be optimized with aircraft performance. So far, almost all work on noise suppression has been experimental, as theoretical developments of the supersonic jet noise theory have been lacking. It has been generally accepted that in the subsonic jet the dominating noise generating mechanism is the turbulent mixing as proposed by Lighthill[1], whereas in the supersonic jet it is an accumulative effect of Mach wave radiation, shock-turbulence interaction and shock unsteadiness, turbulent mixing and nozzle lip radiation. Their presence has been established by shadowgraph and holographic techniques and has been reported by Louis et al.[2] and others. The exact contribution by each of the above noise generating mechanisms to the total supersonic jet noise has not yet been assessed. Mathematically, it is difficult to decouple their contributions because of the complexity of their origins, but by means of specially-designed experiments in which one form of the noise generating mechanism is more pronounced over the other forms, then the dependence of that particular noise generating mechanism on the flow parameters (jet density, velocity and Mach number) of the jet can be studied by varying one flow parameter at a time. Louis et al.[2] propose that by presenting a comparative study of two different nozzle configurations: a rectangular and a circular supersonic nozzle,

each having the same exit Mach number and identical momentum and energy flux, the dependence of each noise generating mechanism on flow parameters can be studied. Both the rectangular and circular nozzles used in Ref. 2 have the same exit Mach number of 2.74 and exit area of 0.154 sq.in. Due to the difference in geometry, the rectangular jet undergoes a rapid deceleration through a system of strong shocks, and the length of the system of shocks (which is a function of the nozzle configuration, jet Mach number and jet pressure ratio) is very much shorter than that in the identical circular jet; also there is less of the turbulence in the shear layer to interact with the system of shocks than in the circular jet. This suggests that shock-induced noise is likely to be more important in the circular or axisymmetric jet than in the rectangular jet; and this is confirmed by shadowgraphic studies which reveal that in the rectangular jet practically no spherical acoustic waves (from shock-turbulence interaction) are seen to radiate from the shock tips, whereas in the identical circular jet the spherical acoustic waves are very prominent. However, it must be cautioned that shadowgraphs respond to the second derivative of the density and as such, the prominent waves detected are those with the largest derivative and not necessarily those with a large sound pressure level. On the other hand, measured sound directivity and propagation direction of Mach waves obtained from shadowgraphs indicate that Mach waves contribute importantly to the noise produced by a rectangular jet. Furthermore, in the near-field, the strength of the Mach wave radiation in the rectangular jet is constant along the direction of propagation of the waves and is independent of the distance from the jet axis. This is because the waves are propagating normal to the long and short axes and form parallel rays. In the circular jet, the Mach waves

are diverging forming a source-like flow field and the strength of the waves falls off like the reciprocal of the distance from the jet axis. Because of this difference in nozzle geometry, the Mach wave radiation is more important in the rectangular jet than in the circular jet where the dominating mode of noise production would be the interaction of the shock with turbulence. The results from Ref. 2 indicate that the total acoustic power from the two nozzles (rectangular nozzle and identical circular nozzle) show different dependence on the jet density ratio and jet velocity ratio. This observation suggests that in the rectangular jet the most prominent noise generating mechanism is the eddy Mach wave type of radiation whereas in the circular jet, shock-turbulence and shock unsteadiness may be the most important type of noise generating mechanism.

From the standpoint of developing a scaling law useful for predicting the total acoustic power of supersonic jets, it is important to find how the flow parameters (jet density ratio and jet velocity ratio), dependency or scaling factors for the total acoustic power vary as a function of different nozzle exit Mach numbers. However, because of the difficulty of building a series of rectangular nozzles with different exit Mach numbers, this is done only for the cylindrical supersonic nozzles. In the meantime, a model for the eddy Mach wave radiation is proposed, using the experimental results from this study and Lighthill's theory for the supersonic jet noise. For the circular jet, a model for the shock-turbulence and shock-pressure fluctuations is proposed using experimental results from this study and Kerrebrock's[3] treatment of shock-turbulence and pressure fluctuation interaction. Shadowgraphs are taken for the purpose of identifying the dominant modes of noise production which have been established in this study and in Ref. 2 as eddy Mach wave radiation, shock turbulence and shock-pressure fluctuation interaction, turbulent mixing

and nozzle lip radiation. As explained earlier, shadowgraphs respond to the second derivative of the density, and as such the waves are weighted against the square of the frequencies and those waves of shorter wavelengths appear to be more prominent on the shadowgraphs.

Supersonic Jet Noise Generating Mechanisms

1.1 Mach-Wave Radiation

These are disturbances convected supersonically in the shear layer and these waves propagate in a highly directional path whose angle to the jet axis is determined by the eddy convective velocity. Generally the mean eddy convective velocity is found to vary from 50% to 70% of the jet exit velocity. Tam[4] considers these waves as instability waves propagating in the shear layer. Shadowgraphs indicate that the sources of the Mach wave radiation originate from near the nozzle lip and extend downstream to the sonic point. This observation agrees with Nagamatsu's acoustic measurements of the near field of a jet.[5] Figure 1 shows a sketch of the model of the supersonic jet and the sources of the acoustic radiation.

1.2 Shock Turbulence Interaction and Shock Unsteadiness

The presence of the shock-turbulence interaction, that is, the interaction of turbulence in the shear layer with the shock tips, is indicated in the shadowgraphs by the spherical waves centered at the shock tips and propagating transverse to the jet axis. Evidently some internal shocks cannot be avoided even when the jet is operating under perfect expansion conditions due to the presence of small perturbations in the starting flow. Small disturbances such as vorticity and pressure fluctuations are generated upstream by the unsteadiness of the shock cells and as these

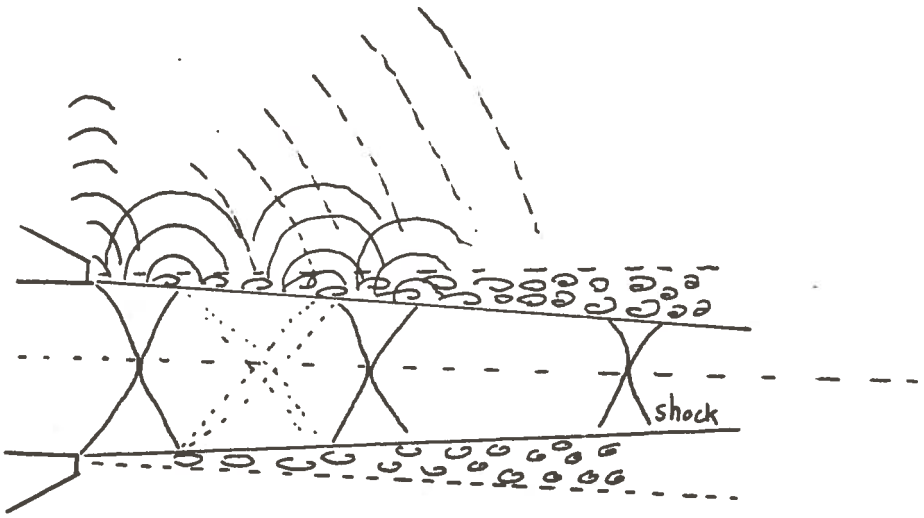

Figure 1: Schematic sketch of a supersonic jet and the noise generating mechanism.

disturbances in the shear layer are propagated downstream, they interact with the shocks creating intense noise. This mechanism is believed to be the main noise generating mechanism in the circular supersonic jet. The sources of these waves would appear to be located at the shock tips where the shear layer interacts with the system of shocks. This observation is consistent with the location of the spherical waves in the shadowgraphs.

1.3 Turbulent Mixing Radiation

The radiation from turbulent mixing is viewed as the dominating mechanism for the noise generation in the subsonic jet and also in the model of the supersonic jet noise proposed by Lighthill.[6] In Nagamatsu's idealized model of the supersonic jet noise[5] the sources of the turbulent mixing radiation is assumed to start from the transition region near the sonic point (M=1) to far downstream where the flow of the jet is subsonic. In the case of the subsonic jet, the strength of the sources of the acoustic radiation (acoustic power output per unit length) is constant for the first 4 or 5 diameters[7] and then decays like $x^{-6}\ell$ where ℓ is the turbulent correlation radius. In the supersonic jet, ℓ is approximately constant over the subsonic portion of the jet and hence for the turbulent mixing, the acoustic power output per unit length decays like x^{-6} along the axial distance in the subsonic portion of the supersonic jet. Based on the present model for the circular supersonic jet noise as resulting from the interaction of turbulence with the shock cells, turbulent mixing is considered to be relatively unimportant in the supersonic jet noise.

1.4 Nozzle Lip Radiation

The presence of the lip wave radiation is not as prominent in the

shadowgraphs of the supersonic circular jet as in the rectangular jet.[8] It has been established experimentally that the thickness of the nozzle lip (which was once thought to have some influence on the separation point of the jet as it exited from the nozzle and hence on the acoustic characteristics of the lip waves) does not influence the acoustic characteristics of the lip waves. The contribution of the lip wave radiation to the total supersonic jet noise power is regarded as not important since there is no indication that the strength of these sources of lip waves is higher than the other noise-producing sources and the lip waves are mainly localized in the region of the nozzle lip.

It appears there is some relationship between Mach waves and lip waves since the Mach waves originate in the turbulent shear layer in the region close to the nozzle where the lip-centered cylindrical waves are also observed. This observation prompts more measurements of the Mach and lip waves concurrently for the low and high temperature conditions. Despite some positive experimental correlation results for the low temperature condition, the relationship, if any, between the Mach and lip waves remains to be established.

Scaling parameters. The basic parameters governing the noise production in a supersonic jet are: the Mach number, the pressure, the temperature (stagnation), the molecular weight and the ratio of the specific heats and the nozzle configuration. Hence, for a given test gas (in this case the test gas is argon) the molecular weight and the ratio of the specific heat are fixed. The three flow parameters remaining, thus, are the Mach number, pressure, and temperature. For different nozzle configurations, the total jet noise power would show different dependence on these three flow parameters since the dominating noise generating mechanism

in each nozzle configuration is different: such as the Mach wave radiation in the rectangular jet and the shock-pressure disturbance and shock turbulence interaction in the circular jet. However, an analysis of Lighthill's jet noise theory and Nagamatsu's supersonic jet noise theory shows that the jet density ratio (ρ_J/ρ_a), the jet velocity ratio (U_J/C_a), and the jet Mach number (M_J) are the more suitable parameters to be used in the scaling law rather than the pressure ratio and the temperature ratio. Also, it can be shown that other important parameters, such as the Reynolds number, can be expressed as a function of these three flow parameters, (ρ_J/ρ_a), (U_J/C_a) and M_J.

1.5 Stagnation Pressure Ratio

The stagnation pressure ratio of the jet determines the level of expansion and hence the strength and length of the system of shocks. It also determines the jet density for a given stagnation temperature. Therefore, the stagnation pressure ratio would to some extent indicate the influence and the importance of the shock-turbulence interaction. Furthermore, the pressure ratio can be expressed as a function of the three selected flow parameters through the isentropic expansion relations and the equation of state.

The exit pressure of the jet is given by

$$\frac{P_J}{P_0} = \left(1 + \frac{\gamma-1}{2} M_J^2\right)^{-\frac{\gamma}{\gamma-1}} \qquad (1\text{-}5\text{-}1)$$

Also

$$\frac{P_a}{P_{0\,perf.}} = \left(1 + \frac{\gamma-1}{2} M_J^2\right)^{-\frac{\gamma}{\gamma-1}} \qquad (1\text{-}5\text{-}2)$$

Therefore,

$$\frac{P_o}{P_{o\ perf.}} = \frac{P_J}{P_a} \qquad (1\text{-}5\text{-}3)$$

where $P_{o\ perf.}$ is the stagnation pressure required to produce perfectly expanded flow at the nozzle exit ($P_J = P_a$) and P_a is the ambient pressure.

From the equation of state for perfect gas

$$\rho_J = \frac{P_J}{\frac{R}{M} T_J} \qquad (1\text{-}5\text{-}4)$$

ρ_J is the jet density at the exit plane of the nozzle,

ρ_a is the density of the ambient air,

P_J is the jet static pressure at the exit plane of the nozzle,

T_J is the jet static temperature at the exit plane of the nozzle,

T_c is the ambient temperature,

R is the universal gas constant, and

M is the molecular weight of the test gas.

$$\therefore \frac{P_o}{P_{o\ perf.}} = \frac{P_J}{P_a} = \text{constant} = \left(\frac{\rho_J}{\rho_a}\right)\left(\frac{T_J}{T_a}\right) \qquad (1\text{-}5\text{-}5)$$

But

$$\frac{T_J}{T_a} \propto \frac{C_J^2}{C_a^2}$$

Therefore, the stagnation pressure ratio

$$\frac{P_o}{P_{o\ perf.}} \propto \left(\frac{\rho_J}{\rho_a}\right) \cdot \left(\frac{C_J}{u_J}\right)^2 \cdot \left(\frac{u_J}{C_a}\right)^2 \qquad (1\text{-}5\text{-}6)$$

$$\propto \left(\frac{\rho_J}{\rho_a}\right) \cdot \frac{1}{M_J^2} \cdot \left(\frac{u_J}{C_a}\right)^2$$

1.6 Reynolds Number Based on the Viscosity of the Ambient Air and Exit Diameter of the Jet

The Reynolds number can be regarded as the ratio of the inertia force over the viscous force, and it is an important consideration in determining the level of turbulence in the jet flow. The Reynolds number for the supersonic jets in this investigation are in the turbulent regime and the jets and especially the shear layer are fully turbulent. In the case of an argon jet discharging into the ambient atmosphere, two Reynolds numbers can be defined: one based on the viscosity of the ambient air and the other based on the viscosity of the jet. An appropriate choice of the characteristic length is the exit diameter of the nozzle. The Reynolds number based on the viscosity of the ambient air is an important parameter in determining the viscous stresses in the shear layer, while the Reynolds number based on the viscosity of the test jet is the important parameter in determining the viscous stresses in the interior of the jet. Basically the viscous stresses in the supersonic jet are contained in two regions: the shear layer and the main core.

The Reynolds number based on the viscosity of the ambient air is defined as

$$Re_{D_a} = \frac{\rho_J u_J D}{\mu_a} \qquad (1\text{-}6\text{-}1)$$

For ambient air, μ_a is constant and D is constant for a given nozzle. Therefore, the parameter can be expressed as

$$Re_{D_a} = \text{Constant} \cdot \left(\frac{\rho_J}{\rho_a}\right) \cdot \left(\frac{u_J}{C_a}\right) \qquad (1\text{-}6\text{-}2)$$

1.7 Reynolds Number Based on the Viscosity of the Test Gas (Argon) and Exit Diameter of the Jet

$$Re_{D_J} = \frac{\rho_J u_J D}{\mu_J} \qquad (1\text{-}7\text{-}1)$$

But for a noble gas such as argon, the viscosity is proportional to the square root of the jet temperature and similarly the velocity of the jet is also proportional to the square root of the jet temperature.

Therefore

$$Re_{D_J} = \text{Constant} \cdot \left(\frac{\rho_J}{\rho_a}\right) \qquad (1\text{-}7\text{-}2)$$

1.8 Stagnation Temperature Ratio

The main influence of the stagnation temperature ratio on the total noise power can be best viewed as the influence of the jet kinetic energy. Since the jet velocity is a function of the stagnation temperature for a given M_J, increasing the stagnation temperature would increase the total kinetic energy of the jet and hence the total acoustic power. The density of the jet is also affected by the jet temperature and the density falls off like the reciprocal of the jet temperature. In the case of a light test gas driving into a heavier gas, instability known as Taylor's

instability will develop and it strongly influences the stability of the shear layer.

$T_{o\ perf.}$ is given by

$$\frac{T_{o\ perf.}}{T_a} = \left(1 + \frac{\gamma-1}{2} M_J^2\right) \tag{1-8-1}$$

and

$$\frac{T_o}{T_J} = \left(1 + \frac{\gamma-1}{2} M_J^2\right) \tag{1-8-2}$$

So

$$\frac{T_o}{T_{o\ perf.}} = \frac{T_J}{T_a} \propto \left(\frac{C_J}{C_a}\right)^2 \tag{1-8-3}$$

$$\propto \left(\frac{C_J}{u_J}\right)^2 \cdot \left(\frac{u_J}{C_a}\right)^2$$

$$\propto \frac{1}{M_J^2} \cdot \left(\frac{u_J}{C_a}\right)^2$$

II. FORMULATION OF THE THEORY ON SUPERSONIC JET NOISE

The present theory is formulated in three parts. Part 1 deals essentially with the Mach wave radiation as the principal noise generating mechanism in the rectangular jet. Part 2 deals with the shock-turbulence and shock-pressure fluctuation interaction as the principal noise generating mechanism in the circular jet. Part 3 is devoted to a complete analysis of the strength of the oblique shocks and the length of the shock cells.

Part 1

2.1 Mach Wave Radiation

Mach waves are weak but finite waves that are produced by small disturbances; they are not the same as Mach lines which have zero strength. Lighthill has regarded these waves as a distribution of weak ballistic shock waves generated by the motion of eddies or disturbances through the atmosphere faster than the atmospheric speed of sound. The governing equations of motion for the eddies are

$$\frac{\partial \rho}{\partial t} + \sum_{i=1}^{3} \frac{\partial (\rho v_i)}{\partial x_i} = 0 \qquad (2\text{-}1\text{-}1)$$

$$\frac{\partial (\rho v_i)}{\partial t} + \sum_{j=1}^{3} \frac{\partial (\rho v_i v_j + \dot{p}_{ij})}{\partial x_j} = 0 \qquad (2\text{-}1\text{-}2)$$

Expressing

$$T_{ij} = \rho v_i v_j + p_{ij} - c_a^2 \rho \delta_{ij} \qquad (2\text{-}1\text{-}3)$$

Then, from the above equations, the following expression is obtained:

$$\frac{\partial^2 \rho}{\partial t^2} - \sum_{i=1}^{3} c_a^2 \frac{\partial^2 \rho}{\partial x_i} = \sum_{i=1}^{3} \sum_{j=1}^{3} \frac{\partial^2 T_{ij}}{\partial x_i \partial x_j} \qquad (2\text{-}1\text{-}4)$$

Using Kirchoff's relation

$$c_a^2 (\rho - \rho_a) = \sum_{i=1}^{3} \sum_{j=1}^{3} \frac{\partial^2}{\partial x_i \partial x_j} \int_V \frac{[T_{ij}]}{4\pi r} \, dV \qquad (2\text{-}1\text{-}5)$$

Equation (2-1-5) is the Lighthill's equation and the bracket [] indicates evaluation at the retarded time $\hat{t} = t - \frac{r}{c_a}$.

Considering only the far field,

$$\frac{\partial}{\partial x_j} [T_{ij}] = - \frac{1}{c_a} \frac{\partial}{\partial t} [T_{ij}] \frac{\partial r}{\partial x_j} \qquad (2\text{-}1\text{-}6)$$

$$= - \frac{1}{c_a} \frac{\partial}{\partial t} [T_{ij}] \frac{x_j}{r} \qquad (2\text{-}1\text{-}7)$$

Therefore, the acoustic far field can be written as

$$\rho - \rho_a = \sum_{i=1}^{3} \sum_{j=1}^{3} \frac{x_i x_j}{4\pi C_a^2 r^3} \int_V \left[\ddot{T}_{ij}\right] d\tau \qquad (2\text{-}1\text{-}8)$$

where $[\ddot{T}]$ is the second time derivative of T_{ij} and the volume of integration is over the entire volume of the eddies. At this point it is worthwhile to examine how to interpret the term T_{ij}. T_{ij} contains the fluctuating Reynolds stresses, $\rho V_i V_j$, the real stresses, p_{ij}, and the stresses in the uniform acoustic medium at rest, $C_a^2 \rho \delta_{ij}$. The only important stresses to be considered are the fluctuating Reynolds stresses which correspond to variable rates of momentum flux across surfaces fixed in the fluctuating fluid flow. These fluctuating stresses are generated by the fluctuating shearing motions of the eddies as the eddies are being convected in the shear layer. In subsonic flow, this mechanism is reduced to the turbulent mixing from which acoustic energy is radiated as quadrupole radiation. In the supersonic jet, the eddies are moving with a convection speed greater than the atmospheric speed of sound and hence most of the acoustic energy is radiated in the forward direction. It is perfectly clear that Lighthill's analysis of subsonic turbulent noise is equally applicable to the Mach wave radiation of the supersonically convecting turbulent eddies.

In order to estimate the integral contribution from the whole jet, the statistical properties of the flow of the eddies must be taken into account. To do so the flow is divided into regions such that strengths of the sources in different regions are uncorrelated. Hence the acoustic

output for a single region is

$$\rho - \rho_a = \sum_{i=1}^{3} \sum_{j=1}^{3} \frac{x_i x_j}{4\pi c_a^2 r^3} V_e \left[\ddot{T}_{ij}\right] \qquad (2\text{-}1\text{-}9)$$

Since the acoustic intensities combine linearly for uncorrelated sources, the total acoustic intensity for the entire volume of jet is

$$\frac{\langle (\rho - \rho_a)^2 \rangle}{\rho_a c_a} = \frac{V_e^2 \left[\overline{\ddot{T}_{ij}^2}\right]}{\rho_a c_a^5 r^2} \qquad (2\text{-}1\text{-}10)$$

where $\left[\overline{\ddot{T}_{ij}^2}\right]$ is a typical mean square fluctuation of T_{ij} and can be rewritten as $\omega^4 \overline{T^2}$ where ω is a typical radian frequency of fluctuation and $\overline{T^2}$ is a typical mean square value of the strength of the source. Therefore, the acoustic power output per unit volume of eddies is

$$\frac{V_e \omega^4 \overline{T^2}}{\rho_a c_a^5} \qquad (2\text{-}1\text{-}11)$$

By dimensional analysis, V_e is proportional to ℓ^3 where ℓ is the mean radius of an eddy and is proportional to d, ω is proportional to $\frac{U}{d}$, and $\overline{T^2}$ is proportional to $(\rho_I J_U^2)^2$ where ρ_I is a typical density of the eddies. Therefore, the acoustic power output per unit volume of the eddies is

proportional to

$$\frac{\left(\frac{\rho_I^2}{\rho_a} \cdot \frac{u_J^8}{d}\right)}{C_a^5} \qquad (2\text{-}1\text{-}12)$$

The density ρ_I of the eddies should be intermediate between ρ_a and ρ_J. Rewriting ρ_I as some function of ρ_J such that the dependence of the acoustic power on the jet density (ρ_J) varies with a power ranging from 1.0 to 2.0 as suggested by the results of Coles[9,10] and Lassiter[11],

$$\rho_I = \rho_J^{\phi_1} \qquad (2\text{-}1\text{-}13)$$

where ϕ_1 varies between 0.5 and 1.0. In general, ϕ_1 is a function of the jet Mach number. The acoustic power output per unit volume of the eddies in a stationary frame is

$$\left(\frac{\rho_J}{\rho_a}\right)^{2\phi_1} \cdot \frac{u_J^8}{C_a^5} \quad \frac{\rho_a}{d} \qquad (2\text{-}1\text{-}14)$$

However, it must be taken into account that the eddies are not stationary but are moving with a mean convective Mach number M_c. The effect of the convection appears in the addition of the term $\left\{(1-M_c \cos\theta)^2 + \left(\frac{\omega l}{C_a}\right)^2\right\}^{-3}$ as has been shown by Ffowcs Williams.[12] Furthermore, by including only moving eddies whose radiation arrives simultaneously and the fact that

the slope of the convected velocity and the signal velocity do not coincide, Ffowcs Williams has shown that there is an additional correction of $\left\{(1-M_c\cos\theta)^2+\left(\frac{\omega l}{C_a}\right)^2\right\}^{1/2}$. Therefore, the acoustic power output per unit volume of the convecting eddies is given by

$$W_e = \left(\frac{\rho_J}{\rho_a}\right)^{2\phi_1} \cdot \frac{\rho_a}{d} \cdot \frac{U_J^8}{C_a^5}\left\{(1-M_c\cos\theta)^2+\left(\frac{\omega l}{C_a}\right)^2\right\}^{-5/2} \quad (2\text{-}1\text{-}15)$$

The peak acoustic power is directed in the direction $\theta = \cos^{-1}\frac{1}{M_c}$ and this is the direction along which the maximum acoustic power is radiated and which the Mach waves appear to be propagating. For the contributions of the Mach wave radiation, the acoustic intensity per unit length of jet by the Mach waves propagating in the θ direction is proportional to

$$\left(\frac{\rho_J}{\rho_a}\right)^{2\phi_1} \rho_a d \frac{U_J^8}{C_a^5}\left\{\left(\frac{\omega l}{C_a}\right)^{-5}\right\} \quad (2\text{-}1\text{-}16)$$

It can be shown that ωl is proportional to the rms turbulent velocity which itself increases less rapidly than U_J. Therefore, ωl would be proportional to some power of U_J,

$$\frac{\omega l}{C_a} \simeq \left(\frac{U_J}{C_a}\right)^{\phi_2} \quad (2\text{-}1\text{-}17)$$

where ϕ_2 is a function of jet Mach number (U_J/C_J) and the velocity ratio

(C_J/C_a) and to a lesser degree on the Reynolds number.

From equations (2-1-16) and (2-1-17) the acoustic intensity of the Mach waves is obtained as

$$\left(\frac{\rho_J}{\rho_a}\right)^{2\phi_1} \cdot \rho_a d \left(\frac{u_J}{C_a}\right)^{8-5\phi_2} \cdot C_a^3 \qquad (2\text{-}1\text{-}18)$$

Since ρ_a, d, C_a are constants for a given nozzle and ambient condition, the acoustic intensity of the Mach wave radiation is proportional to

$$\left(\frac{\rho_J}{\rho_a}\right)^{2\phi_1} \cdot \left(\frac{u_J}{C_a}\right)^{8-5\phi_2} \qquad (2\text{-}1\text{-}19)$$

In general, the acoustic intensity of the Mach waves varies as a function of the axial distance along the jet. This is due to the fact that the eddies are being elongated as they are convected downstream and tend to break up into smaller eddies to conserve vorticity. As suggested by Nagamatsu, the acoustic intensity of the Mach waves would vary linearly with distance. Physically, it means that more eddies are formed downstream or that more different eddies become correlated downstream and their amplitudes of the pressure fluctuations combine linearly to give a higher acoustic intensity. Using this assumption and the fact that the Mach waves do not extend beyond the sonic point, the total acoustic power from the supersonic jet is obtained by integrating the acoustic power output per unit length from the Mach waves over the length of the supersonic region.

The contribution from the turbulent mixing noise over the subsonic region of the jet is obtained by integrating from the sonic point to a point far downstream. It has been noted that the acoustic power output per unit length in the subsonic region of the supersonic jet decays like x^{-6}. Nagamatsu has assumed the empirical relation for the length of the supersonic region of the perfectly expanded jet to be

$$L_S = 5 M_J^2 + 0.8 \qquad (2\text{-}1\text{-}20)$$

This is not the case in the present experiment since the jets are operated under different expanded conditions, and Price's[13] result for argon jets under different pressure ratios is more applicable to the present analysis.

Price gives the spatial distance between two shock cells as

$$\frac{S}{d} = 1.2 \left(R^* - R_c^* \right)^{0.35} \qquad (2\text{-}1\text{-}21)$$

where R^* = pressure ratio = $\frac{P_o}{P_a}$

R_c^* = critical pressure ratio = 2.39 for argon

s = shock separation

d = nozzle diameter.

$$R^* = \frac{P_o}{P_a} = \frac{P_o}{P_{o\ perf.}} \cdot \frac{P_{o\ perf.}}{P_a}$$

$$\equiv \frac{P_J}{P_a} \left(1 + \frac{\gamma - 1}{2} M_J^2 \right)^{\gamma/\gamma - 1} \qquad (2\text{-}1\text{-}22)$$

$$\frac{s}{d} = 1.2\left[\frac{P_J}{P_a}\left(1+\frac{\gamma-1}{2}M_J^2\right)^{\gamma/\gamma-1} - 2.39\right]^{0.35} \qquad (2\text{-}1\text{-}23)$$

Assuming there are n shock cells in the supersonic length, then the supersonic length is given by

$$L_s^* = 1.2n\left[\frac{P_J}{P_a}\left(1+\frac{\gamma-1}{2}M_J^2\right)^{\gamma/\gamma-1} - 2.39\right]^{0.35} \qquad (2\text{-}1\text{-}24)$$

The value of n can be easily determined from equations (2-1-20) and (2-1-23):

$$n = \frac{5M_J^2 + 0.8}{1.2\left[\left(1+\frac{\gamma-1}{2}M_J^2\right)^{\gamma/\gamma-1} - 2.39\right]^{0.35}} \qquad (2\text{-}1\text{-}25)$$

Since both equations (2-1-20) and (2-1-23) are established empirically and n must be an integer, the value of n determined from equation (2-1-25) is rounded to the nearest integer to give the exact number of shock cells in the supersonic length.

Alternatively, the constant in Price's empirical relation for s/d in equation (2-1-21) and the constant for L_s in equation (2-1-20) are corrected so that n is an integer.

For the supersonic region $\left(0 \leq \frac{x}{d} \leq L_s^*\right)$ the acoustic output per unit exit diameter is assumed to be

$$W_e = f_o(M_J) + \frac{g_o(M_J) - f_o(M_J)}{L_s^*} \frac{x}{d} \qquad (2\text{-}1\text{-}26)$$

The above expression is similar to the derivation given by Nagamatsu except that in the present case

$$f_o(M_J) = K_1 \left(\frac{\rho_J}{\rho_a}\right)^{2\phi_1} \cdot \left(\frac{u_J}{C_a}\right)^{8-5\phi_2} M_J^{-\alpha} \qquad (2\text{-}1\text{-}27)$$

$$g_o(M_J) = K_1 \left(\frac{\rho_J}{\rho_a}\right)^{2\phi_1} \left(\frac{u_J}{C_a}\right)^{8-5\phi_2} M_J^{-\beta} \qquad (2\text{-}1\text{-}28)$$

The motivation for writing $f_o(M_J)$ as equation (2-1-27) is to give the acoustic output per unit exit diameter at the nozzle exit which is a function of the jet Mach number. $g_o(M_J)$ gives the slope of the distance of the acoustic output per unit exit diameter along the axial distance. K_1 is a constant and is the same for all jets of the same diameter and operating in the same ambient conditions; α and β are variables to be determined from experimental results, and in general α and β are functions of jet Mach numbers only.

The total contribution of the Mach wave radiation from the supersonic

region is obtained by integrating over the length from $0 \leq \frac{x}{d} \leq L_s^*$:

$$\overline{W_e} = f_o(M_J) L_s^* + \frac{g_o(M_J) - f_o(M_J)}{L_s^*} \frac{L_s^{*2}}{2}$$

$$= \frac{L_s^*}{2} \left[f_o(M_J) + g_o(M_J) \right] \qquad (2\text{-}1\text{-}29)$$

Substituting equations (2-1-24), (2-1-27) and (2-1-28) in the above equation

$$\overline{W_e} = 1.2n K_1 \left(\frac{\rho_J}{\rho_a}\right)^{2\phi_1} \left(\frac{U_J}{C_a}\right)^{8-5\phi_2} \frac{M_J^{-\alpha} + M_J^{-\beta}}{2} \times$$

$$\times \left[\frac{P_J}{P_a} \left(1 + \frac{\gamma-1}{2} M_J^2\right)^{\gamma/\gamma-1} - 2.39 \right]^{0.35} \qquad (2\text{-}1\text{-}30)$$

Rewriting P_J/P_a as $(\rho_J/\rho_a) \cdot (U_J/C_a)^2$, equation (2-1-30) becomes

$$\overline{W_e} = 1.2n K_1 \left(\frac{\rho_J}{\rho_a}\right)^{2\phi_1} \left(\frac{U_J}{C_a}\right)^{8-5\phi_2} \left(\frac{M_J^{-\alpha} + M_J^{-\beta}}{2}\right) \times$$

$$\times \left[\left(\frac{\rho_J}{\rho_a}\right) \left(\frac{U_J}{C_a}\right)^2 \left(1 + \frac{\gamma-1}{2} M_J^2\right)^{\gamma/\gamma-1} - 2.39 \right]^{0.35} \qquad (2\text{-}1\text{-}31)$$

The variables ϕ_1, ϕ_2, α and β are determined experimentally.

For a given nozzle, M_j is fixed and varying the jet density ratio and jet velocity ratio one at a time, the variables ϕ_1 and ϕ_2 are determined from the scaling law obtained experimentally. Therefore, the total acoustic power generated by means of Mach wave radiation is proportional to the jet density ratio ρ_J/ρ_a to the power $(2\phi_1 + 0.35)$, and to the jet velocity ratio U_J/C_a to the power $(8 - 5\phi_2 + 0.70)$. (A similar analysis for the case of an air-jet is given in Appendix A.)

Mach wave radiation appears to be the most important noise generating mechanism in the rectangular supersonic jet and the total acoustic power from the rectangular jet would vary as $(2\phi_1 + 0.35)$ power of the density and $(8 - 5\phi_2 + 0.70)$ power of the velocity.

Lighthill's eight-power law of the jet velocity in the subsonic jet can be derived from the above analysis. When the jet is subsonic, the eddies are moving with subsonic speed and turbulent mixing becomes the most important mechanism. The functions $f_o(M_J)$ and $g_o(M_J)$ are the same since α and β approach zero as M_J approaches 1.0 as indicated by Nagamatsu et al.[14] The acoustic power output would be reduced to

$$\left(\frac{\rho_J}{\rho_a}\right)^{2\phi_1} \left(\frac{U_J}{C_a}\right)^{8-5\phi_2}$$

For $\phi_1 = 0.5$ and $\phi_2 = 0$, the above relation is reduced to Lighthill's results for the acoustic power output of the subsonic jet.

Part 2

2.2 Shock-Turbulence and Shock-Pressure Fluctuations Interaction

In Part 1 the generation of noise by relatively strong vorticity or eddies is considered. On the other hand, even if the disturbances such as fluctuations of pressure, entropy and vorticity are weak, they will interact

if carried through a region of high gradients in the mean flow quantities since the interaction terms again become large in this region. The three common flow phenomena in which very large gradients are encountered are shock waves, flame fronts and shear layers. In this study, only the interactions of the pressure and vorticity disturbances with the shock waves are considered. These small disturbances, pressure and vorticity are ordinarily random, and only the statistical properties of the disturbances can be specified, and hence only the influence of the shock wave on these properties can be determined. It will be assumed that the input disturbances are isotropic and the shock wave is an infinite plane, separating two semi-infinite regions of uniform flow perturbed by the small disturbance fields. The small disturbances can be weak turbulent eddies in the shear layer or weak pressure fluctuations generated by the unsteadiness of the shock cells in the jet. The present analysis of the interaction of small disturbances with the shock waves is attributed to Kerrebrock.[3]

Summary of Kerrebrock's theory on the interaction of flow discontinuities with small disturbances: governing equations of the fluid. Neglecting the effects of viscosity and heat conduction, the equations governing the fluid are:

Continuity
$$\frac{\partial \rho^*}{\partial t} + \nabla\cdot(\rho^* \underline{u}^*) = 0 \qquad (2\text{-}2\text{-}1)$$

Momentum
$$\rho^* \frac{Du^*}{Dt} + \nabla p^* = 0 \qquad (2\text{-}2\text{-}2)$$

Energy
$$\frac{Ds^*}{Dt} = 0 \qquad (2\text{-}2\text{-}3)$$

State
$$p^* = \rho^* R T^* \qquad (2\text{-}2\text{-}4)$$

For small disturbances, introduce the new variables

$$u_1 = u_1^* - U$$
$$u_2 = u_2^*$$
$$u_3 = u_3^*$$
$$p = p^* - P$$
$$\delta\rho = \rho^* - \rho$$
$$s = s^* - S_o$$

in the above equations. The resulting set of equations is

$$\left(\frac{\partial}{\partial t} + U \frac{\partial}{\partial x_1} \right) \underline{u} + \frac{1}{\rho} \nabla p = 0 \qquad (2\text{-}2\text{-}5)$$

$$\frac{1}{a^2} \left(\frac{\partial}{\partial t} + U \frac{\partial}{\partial x_1} \right)^2 p - \nabla^2 p = 0 \qquad (2\text{-}2\text{-}6)$$

$$\left(\frac{\partial}{\partial t} + U \frac{\partial}{\partial x_1} \right) s = 0 \qquad (2\text{-}2\text{-}7)$$

Taking the curl of equation (2-2-5) and letting the vorticity associated with the disturbance be $\underline{\Omega} = \nabla X \underline{u}$, the equation governing the vorticity is

$$\left(\frac{\partial}{\partial t} + U \frac{\partial}{\partial x_1} \right) \underline{\Omega} = 0 \qquad (2\text{-}2\text{-}8)$$

The disturbance fields can be represented by Fourier integrals in

terms of the stationary coordinate system as follows:

$$\frac{u}{U} = \int e^{i[k_1(x_1 - Ut) + k_2 x_2 + k_3 x_3 + \omega t]} \, dZ(\underline{k}, \omega)$$

$$\frac{p}{p} = \int e^{i[k_1(x_1 - Ut) + k_2 x_2 + k_3 x_3 + \omega t]} \, dZ_p(\underline{k}, \omega) \qquad (2\text{-}2\text{-}10)$$

$$\frac{s}{C_p} = \int e^{i[k_1(x_1 - Ut) + k_2 x_2 + k_3 x_3 + \omega t]} \, dZ_s(\underline{k}, \omega) \qquad (2\text{-}2\text{-}11)$$

Substituting the Fourier integrals into the differential equations (2-2-6) to (2-2-8), the following expressions are obtained:

For the pressure field

$$\omega^2 = a^2(k_1^2 + k_2^2 + k_3^2)$$

$$\omega = \pm a \underline{k} \qquad (2\text{-}2\text{-}12)$$

and for the vorticity and entropy fields

$$\omega = 0 \qquad (2\text{-}2\text{-}13)$$

Part of the velocity field is associated with the pressure field (Eq. 2-2-5) and part with the vorticity field (Eq. 2-2-8). The disturbance fields upstream of the discontinuity (shock wave) are

expressed as follows:

Upstream of S,

$$\frac{u_v}{U} = \int e^{i[k_1(x_1 - Ut) + k_2 x_2 + k_3 x_3]} \, d\underline{Z}_v(\underline{k}) \qquad (2\text{-}2\text{-}14)$$

$$\frac{s}{c_p} = \int e^{i[k_1(x_1 - Ut) + k_2 x_2 + k_3 x_3]} \, d\underline{Z}_s(\underline{k}) \qquad (2\text{-}2\text{-}15)$$

$$\frac{p}{\bar{p}} = \int e^{i[k_1(x_1 - Ut) + k_2 x_2 + k_3 x_3]} \, d\underline{Z}_p(\underline{k}) \qquad (2\text{-}2\text{-}16)$$

$$\frac{u_p}{U} = \int e^{i[k_1(x_1 - Ut) + k_2 x_2 + k_3 x_3 - a\underline{k}t]} \frac{\underline{k}}{k} \, d\underline{Z}_p(\underline{k}) \qquad (2\text{-}2\text{-}17)$$

In order to simplify the boundary conditions at the discontinuity it is transformed to a coordinate system in which the discontinuity appears normal to the stream velocity as indicated in Fig. 2.

$$x_1 = \xi \sin\theta + \eta \cos\theta + Ut \cos^2\theta$$

$$x_2 = -\xi \cos\theta + \eta \sin\theta + Ut \cos\theta \sin\theta$$

$$k_1 = k_1 \sin\theta + k_2 \cos\theta$$

$$K_2 = -k_1 \cos\theta + k_2 \sin\theta$$

$$k_3 = k_3 \qquad , \qquad U = \frac{U_n}{\sin\theta}$$

In terms of the new coordinate system, the disturbance fields are written as follows:

Upstream of the discontinuity,

$$\frac{u_v}{U_n} = \int e^{i[k_1(\xi - U_n t) + k_2 \eta + k_3 x_3]} \, d\underline{Z}_v(\underline{k}) \Big/ \sin\theta \qquad (2\text{-}2\text{-}18)$$

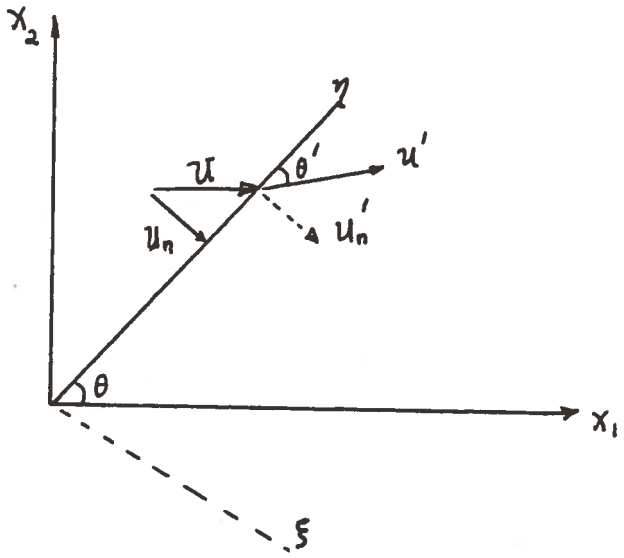

Figure 2: Transformation from case of oblique discontinuity in x_1, x_2, x_3 coordinate system to case of normal discontinuity in §, η, and x_3 coordinate system.

$$\frac{s}{C_p} = \int e^{i[k_1(\xi - U_n t) + k_2\eta + k_3 x_3]} \, d\underline{Z}_s(k) \tag{2-2-19}$$

$$\frac{p}{P} = \int e^{i[k_1(\xi - U_n t) + k_2\eta + k_3 x_3]} \, d\underline{Z}_p(k) \tag{2-2-20}$$

$$\frac{u_p}{U_n} = \int e^{i[k_1(\xi - U_n t) + k_2\eta + k_3 x_3 - akt]} \frac{\underline{k}}{k} \, d\underline{Z}_p(\underline{k}) \Big/ \gamma M_n \tag{2-2-21}$$

For the downstream side of the discontinuity

$$\frac{u'_v}{U'_n} = \int e^{i[k'_1(\xi - U'_n t) + k'_2\eta + k'_3 x_3]} \, d\underline{Z}'_v(\underline{k}) \Big/ \sin\theta' \tag{2.2.22}$$

$$\frac{s'}{C_p} = \int e^{i[k'_1(\xi - U'_n t) + k'_2\eta + k'_3 x_3]} \, d\underline{Z}'_s(\underline{k}) \tag{2.2.23}$$

$$\frac{p'}{P} = \int e^{i[k'_1(\xi - U'_n t) + k'_2\eta + k'_3 x_3]} \, d\underline{Z}'_p(\underline{k}) \tag{2-2-24}$$

$$\frac{u'_p}{U'_n} = \int e^{i[k'_1(\xi - U'_n t) + k'_2\eta + k'_3 x_3 - a'k't]} \frac{\underline{k}}{k} \, d\underline{Z}'_p(\underline{k}) \Big/ \gamma M'_n \tag{2-2-25}$$

The matching of wave numbers may be divided into two cases:

1) The known upstream disturbance consists only of convected vorticity and entropy.

$$k'_2 = k_2$$

$$k'_3 = k_3$$

$$k_4 = \sqrt{k_2 + k_3}$$

Matching of the time dependence yields for the convected downstream disturbance

$$k'_1 = mk_1 \tag{2-2-26}$$

where $m = U_n/U'_n$,

and for the downstream pressure disturbance

$$k'_{1p}\, U'_n + k'_p\, a' = k_1 \qquad (2\text{-}2\text{-}27)$$

and

$$\frac{k'_{1p}}{k_1} = \frac{-m M'^2_n}{1-M'^2_n}\left[1 - \frac{1}{M'_n}\sqrt{1 - \frac{1-M'^2_n}{m^2 M'^2_n}\left(\frac{k_4}{k_1}\right)^2}\right] \qquad (2\text{-}2\text{-}28)$$

and for the upstream pressure disturbance

$$\frac{k_{1pR}}{k_1} = \frac{-M_n^2}{1-M_n^2}\left[1 + \frac{1}{M_n}\sqrt{1 - \frac{1-M_n^2}{M_n^2}\left(\frac{k_4}{k_1}\right)^2}\right] \qquad (2\text{-}2\text{-}29)$$

The downstream pressure waves are not attenuated if

$$\frac{1-M'^2_n}{m^2 M'^2_n}\left(\frac{k_4}{k_1}\right)^2 \leq 1 \qquad (2\text{-}2\text{-}30)$$

2) For the second case, the known upstream disturbance consists only of pressure waves and there can be no upstream convected disturbance. For the downstream convected disturbances

$$k'_1 = m\left(k_{1p} + \frac{1}{M_n}\sqrt{k_{1p}^2 + k_4^2}\right) \qquad (2\text{-}2\text{-}31)$$

and the resulting downstream pressure wave

$$\frac{k'_{1p}}{k'_1} = \frac{-M_n^2}{1-M_n'^2}\left[1 - \frac{1}{M'_n}\sqrt{1 - \frac{1-M_n'^2}{M_n'^2}\left(\frac{k_4}{k_1}\right)^2}\right] \qquad (2\text{-}2\text{-}32)$$

For the reflected upstream pressure wave,

$$\frac{k_{1pR}}{k'_1} = \frac{-2M_n^2 - M_n(1+M_n^2)}{m(1-M_n^2)\left(1 + M_n\frac{k_{1p}}{k_p}\right)} \qquad (2\text{-}2\text{-}33)$$

Matching the velocity conditions yields

$$\frac{U'_t}{U'_n} = m\frac{U_t}{U_n} \qquad (2\text{-}2\text{-}34)$$

where U_t is the tangential velocity component.

By assuming that the discontinuity is disturbed so that its angle to the r axis is σ and that the disturbance propagates in the r direction at the same velocity, V, as the upstream disturbance, Kerrebrock obtained the following expressions for

$$\frac{u'_n}{U'_n} \; , \quad \frac{p'}{P'} \; , \quad \frac{s'}{C_p} \; ;$$

$$\frac{u'_1}{U'_n} = b_1\frac{u_1}{U_n} + b_2\frac{s}{C_p} + b_3\frac{p}{P} + (m-b_1)\frac{V}{U_n}\sigma \qquad (2\text{-}2\text{-}35)$$

$$\frac{u'_{r1}}{U'_n} = m\frac{u_r}{U_n} + (1-m)\sigma$$

$$\frac{p'}{P'} = b_4\frac{u_1}{U_n} + b_5\frac{s}{C_p} + b_6\frac{p}{P} - b_4\frac{V}{U_n}\sigma \qquad (2\text{-}2\text{-}36)$$

$$\frac{s'}{C_p} = b_7\frac{u_1}{U_n} + b_8\frac{s}{C_p} + b_9\frac{p}{P} - b_7\frac{V}{U_n}\sigma \qquad (2\text{-}2\text{-}37)$$

with

$$\left.\begin{aligned}
\frac{u_1}{U_n} &= \frac{dZ_{1v}}{\sin\theta} - C_{1I}\frac{k_{1pI}}{k_4}dZ_{pI} - C_{1R}\frac{k_{1pR}}{k_4}dZ_{pR} \\
\frac{s}{C_p} &= dZ_s \\
\frac{p}{P} &= dZ_{pI} + dZ_{pR} \\
\frac{u_r}{U_n} &= -\frac{k_{1v}}{k_4}\frac{dZ_{1v}}{\sin\theta} - C_{1I}dZ_{pI} - C_{1R}dZ_{pR} \\
\sigma &= dZ_\sigma
\end{aligned}\right\} \qquad (2\text{-}2\text{-}38)$$

and

$$\left.\frac{u'_1}{U'_n} = \frac{dZ'_{1v}}{\sin\theta'} - C_2\frac{k'_{1p}}{k_4}dZ'_p\right]$$

$$\frac{s'}{C_p} = dZ'_s$$

$$\frac{p'}{P'} = dZ'_p$$

$$\frac{u'_r}{U'_n} = -\frac{k'_{IV}}{k_4}\frac{dZ'_{IV}}{\sin\theta'} - C_2\, dZ'_p \qquad (2\text{-}2\text{-}39)$$

where

$$C_1 = -\frac{1}{\gamma M_n}\frac{k_4}{k_p}$$

$$C_2 = -\frac{1}{\gamma M'_n}\frac{k_4}{k'_p}$$

and the subscripts I and R mean incident and reflected.

Since in this case, the discontinuity is a shock wave, the following relations are obtained

$$m = \frac{U_n}{U'_n} = \frac{\frac{\gamma+1}{2} M_n^2}{1 + \frac{\gamma-1}{2} M_n^2} \qquad (2\text{-}2\text{-}40)$$

$$\frac{\delta T}{T} = \frac{\delta s}{C_p} + \frac{\gamma-1}{\gamma}\frac{\delta p}{P} \qquad (2\text{-}2\text{-}41)$$

$$\frac{p'}{\bar{p}'} = \left(\frac{4\gamma m}{\gamma+1} M_n'^2\right)\frac{u_n}{U_n} - \left(\frac{2\gamma m}{\gamma+1} M_n'^2\right)\frac{s}{C_p}$$

$$+ \left(1 - 2\frac{\gamma-1}{\gamma+1} m M_n'^2\right)\frac{p}{\bar{p}} \qquad (2\text{-}2\text{-}42)$$

$$\frac{s'}{C_p} = \left[\frac{4m}{\gamma+1} M_n'^2 - 2\left(1 - \frac{\gamma-1}{\gamma+1} m\right)\right]\frac{u_n}{U_n}$$

$$-\left[\frac{2m}{\gamma+1} M_n'^2 - 2 + \frac{\gamma-1}{\gamma+1} m\right]\frac{s}{C_p} + \frac{\gamma-1}{\gamma}\left[1 - \frac{\gamma-1}{\gamma+1} m - \frac{2m}{\gamma+1} M_n'^2\right]\frac{p}{\bar{p}} \qquad (2\text{-}2\text{-}43)$$

The following expressions for b_i's can be obtained by comparing equations (2-2-35) to (2-2-43):

$$\begin{aligned}
b_1 &= -b_2 + 1 \\
b_2 &= 1 - \frac{\gamma-1}{\gamma+1} m \\
b_3 &= \frac{\gamma-1}{\gamma} b_2 \\
b_4 &= \frac{4\gamma m}{\gamma+1} M_n'^2 \\
b_5 &= -\frac{1}{2} b_4 \\
b_6 &= 1 - \frac{\gamma-1}{2\gamma} b_4 \\
b_7 &= \frac{1}{\gamma} b_4 - 2b_2 \\
b_8 &= -\frac{1}{2\gamma} b_4 + b_2 + 1 \\
b_9 &= -\frac{\gamma-1}{2\gamma^2} b_4 + \frac{\gamma-1}{\gamma} b_2
\end{aligned} \qquad (2\text{-}2\text{-}44)$$

Also, for the shock wave, $dZ_{pR} = 0$.

By assuming isotropic disturbances, the statistical properties of the input disturbance fields can be specified by

$$\overline{q_i^2} = \int T_i^{j*} T_i^{j} \, \Phi_{jj}(\underline{k}_j) \, d\underline{k}_j \qquad (2\text{-}2\text{-}45)$$

where $\overline{q_i^2} = \overline{\left(\frac{u_{iw}}{U_n}\right)^2}$ for the vorticity field

$= \overline{\left(\frac{p}{P}\right)^2}$ for the pressure field.

The connection between the representation of the input disturbance fields given by equation (2-2-14) through (2-2-16) and the statistical representation in terms of the spectral tensor Φ_{ii} is

$$\Phi_{ii}(\underline{k}) \, d\underline{k} = \overline{dZ_i^*(\underline{k}) \, dZ_i(\underline{k})} \qquad (2\text{-}2\text{-}46)$$

For the downstream disturbance fields, the statistical properties can be similarly represented and the connection between the representation of the perturbed downstream disturbance fields [equations (2-2-22) through (2-2-25)] and the statistical representation in terms of the spectral tensor $\Phi'_{ii}(\underline{k}')$ is

$$\Phi'_{ii}(\underline{k}') \, d\underline{k}' = \overline{dZ_i^*(\underline{k}') \, dZ_i(\underline{k}')}$$

$$= \overline{\left[T_i^{j*} \, dZ_j^*(\underline{k}_j)\right]\left[T_i^{k} \, dZ_k(\underline{k}_k)\right]} \qquad (2\text{-}2\text{-}47)$$

The transfer functions can be expressed in spherical polar coordinates

by letting

$$k_1 = k \text{ Cos } \theta$$

$$k_2 = k \text{ Sin } \Theta \text{ Sin } \psi$$

$$k_3 = k \text{ Sin } \Theta \text{ Cos } \psi$$

$$k_4 = k \text{ Sin } \Theta$$

$$J\left(\frac{\underline{k}}{k, \Theta, \psi}\right) = k^2 \text{Sin}^2 \Theta \qquad (2\text{-}2\text{-}48)$$

J is the Jacobian of the $\underline{k}$, k, Θ, ψ. The spectral tensor for the isotropic vorticity field is given by

$$\Phi_{vv} = \frac{E(k_v)}{4\pi U_n^2 k_v^2} \text{Sin}^2 \Theta \qquad (2\text{-}2\text{-}49)$$

The total sound generated downstream by the interaction of the shock with vorticity and pressure disturbance inputs can be expressed in the form of

$$\overline{\left(\frac{p'}{P'}\right)^2} = \frac{1}{2U_n^2} \int_0^\infty E(k_v) dk_v \int T_p^{v*} T_p^{v} \text{Sin}^3 \Theta \, d\Theta$$

$$+ 2\pi \int_0^\infty G_p(k_p) k_p^2 dk_p \int T_p^{p*} T_p^{p} \text{Sin} \Theta \, d\Theta \qquad (2\text{-}2\text{-}50)$$

The term $\int_0^\infty E(k_v) dk_v$ is the upstream mean square value of the vorticity

fluctuation $\overline{(\frac{u_{1v}}{U_n})^2}$ and $4\pi \int_0^\infty G_p(k_p) k_p^2 \, dk_p$ is the upstream mean square value of the pressure fluctuations $\overline{(\frac{p}{\bar{p}})^2}$. Therefore

$$\overline{\left(\frac{p'}{\bar{p}'}\right)^2}_{\text{sound}} = \frac{3}{4}\overline{\left(\frac{u_{1r}}{U_n}\right)^2}\int_0^{\theta_{cl}} T_p^{v*} T_p^{v} \sin^3\theta \, d\theta + \frac{1}{2}\overline{\left(\frac{p}{\bar{p}}\right)^2}\int_0^{\theta_{cl}} T_p^{p*} T_p^{p} \sin\theta \, d\theta \qquad (2\text{-}2\text{-}51)$$

The transfer functions T_p^{v*}, T_p^{v}, T_p^{p*}, T_p^{p} are calculated from the relations of dZ_is and the properties of the shock. For convenience, define average values of the transfer functions by

$$\overline{\left(\frac{p'}{\bar{p}'}\right)^2}_{\text{sound}} = \overline{S_p^{v2'}}\,\overline{\left(\frac{u_{1r}}{U_n}\right)^2} + \overline{S_p^{p2'}}\,\overline{\left(\frac{p}{\bar{p}}\right)^2} \qquad (2\text{-}2\text{-}52)$$

Kerrebrock has evaluated the average transfer functions for $\overline{S_p^{v2'}}$ and $\overline{S_p^{p2'}}$ for $\gamma = 1.4$. The upstream pressure disturbance is attenuated on interaction with the shock and the analysis indicates that shock-pressure fluctuation interaction may not be as important as the shock-turbulence interaction. For the shock-turbulence interaction, the average transfer function $\overline{S_p^{v2'}}$ as derived by Kerrebrock[3] for m approaching 1 is given by

$$\overline{S_p^{v'}} = \left(\frac{8}{5}\right)^{1/2} \frac{\gamma}{\gamma+1}\left(\frac{\gamma+1}{2}\right)^{1/4}(m-1)^{1/4} + \theta(m-1)^{5/4} \qquad (2\text{-}2\text{-}53)$$

For (m-1) approaching zero, we can neglect the term $(m-1)^{5/4}$.

The sound generated downstream of the shock is then

$$\overline{\left(\frac{p'}{P'}\right)^2}_{\text{sound}} = \left[\frac{8}{5}\frac{\gamma^2}{(\gamma+1)^2}\left(\frac{\gamma+1}{2}\right)^{1/2}(m-1)^{1/2}\right]\overline{\left(\frac{u_{1v}}{U_n}\right)^2} \qquad (2\text{-}2\text{-}54)$$

Since (m-1) is given by

$$(m-1) = \frac{\frac{\gamma+1}{2}M_n^2}{1+\frac{\gamma-1}{2}M_n^2} - 1 \qquad (2\text{-}2\text{-}55)$$

For m approaching 1, $M_n \to 1$ and let $M_n = 1 + \varepsilon$ and $\varepsilon \ll 1$:

$$(m-1) = \frac{4}{\gamma+1}\epsilon\left[1 - \frac{2(\gamma-1)}{\gamma+1}\epsilon\right]$$

$$= \frac{4}{\gamma+1}\epsilon \qquad (2\text{-}2\text{-}56)$$

Therefore, equation (2-2-54) becomes

$$\overline{\left(\frac{p'}{P'}\right)^2}_{\text{Sound}} = \left[\frac{8}{5}\sqrt{2}\left(\frac{\gamma}{\gamma+1}\right)^2(M_n-1)^{1/2}\right]\overline{\left(\frac{u_{1v}}{U_n}\right)^2} \qquad (2\text{-}2\text{-}57)$$

Furthermore, the strength of the shock given by M_n can be calculated from oblique shock theory. From Liepman and Roshko[15], the expression for the oblique shock from overexpanded jets is

$$\frac{P_a - P_j}{P_a} = \frac{2\gamma}{\gamma+1}\left(M_n^2 - 1\right) \tag{2-2-58}$$

$$\left(M_n^2 - 1\right) = \frac{\gamma+1}{2}\left(1 - \frac{P_j}{P_a}\right)$$

For M_n near 1, $(M_n^2 - 1) \simeq 2(M_n - 1)$, so that

$$\left(M_n - 1\right) = \frac{\gamma+1}{4\gamma}\left(1 - \frac{P_j}{P_a}\right) \tag{2-2-59}$$

and

$$\overline{\left(\frac{p'}{P'}\right)^2}_{\text{sound}} = \left[\frac{8}{5}\cdot\frac{1}{\sqrt{2}}\left(\frac{\gamma}{\gamma+1}\right)^{3/2}\left(1 - \frac{P_j}{P_a}\right)^{1/2}\right]\overline{\left(\frac{u_{1r}}{U_n}\right)^2} \tag{2-2-60}$$

For the case of the underexpanded jet, $\overline{\left(\frac{p'}{P'}\right)^2}_{\text{sound}}$ can be written

$$\overline{\left(\frac{p'}{P'}\right)^2}_{\text{sound}} = \left[\frac{8}{5}\frac{1}{\sqrt{2}}\left(\frac{\gamma}{\gamma+1}\right)^{3/2}\left(\frac{P_j}{P_a} - 1\right)^{1/2}\right]\overline{\left(\frac{u_{1r}}{U_n}\right)^2} \tag{2-2-61}$$

Equation (2-2-61) implies that when $P_J = P_a$, no acoustic power is radiated from the interaction of the turbulence with the shock since M_n is equal to 1 and the shock is now a Mach line. However, it must be remembered that there is still acoustic power radiated from the eddy Mach waves, and as such eddy Mach wave radiation becomes the dominant noise generating mechanism in the perfectly expanded supersonic circular jet. It is difficult to obtain a perfectly expanded supersonic jet since any perturbations in the starting flow are going to create shocks at the nozzle exit. Therefore, the acoustic intensity generated by the jet due to the interaction of turbulence with a single shock is simply

$$I_{sound} = \overline{\left(\frac{p'}{P'}\right)^2}_{Sound} \times \frac{1}{\rho_a C_a}$$

$$= \frac{1}{\rho_a C_a}\left[\frac{8}{5}\frac{1}{\sqrt{2}}\left(\frac{\gamma}{\gamma+1}\right)^{3/2}\left(\frac{P_j}{P_a}-1\right)^{1/2}\right]\overline{\left(\frac{u_{ir}}{U_n}\right)^2} \qquad (2\text{-}2\text{-}62)$$

But $\frac{P_J}{P_a} \propto \left(\frac{\rho_J}{\rho_a}\right)\left(\frac{1}{M_j^2}\right)\left(\frac{U_J}{C_a}\right)^2$ as in equation (1-5-6):

$$I_{sound} = \frac{1}{\rho_a C_a}\left\{\frac{8}{5}\frac{1}{\sqrt{2}}\left(\frac{\gamma}{\gamma+1}\right)^{3/2}\left[\frac{\rho_J}{\rho_a}\cdot\frac{B_o}{M_j^2}\cdot\left(\frac{u_J}{C_a}\right)^2-1\right]^{1/2}\right\}\times \qquad (2\text{-}2\text{-}63)$$

$$\times \overline{\left(\frac{u_{ir}}{U_n}\right)^2}$$

where B_o is a constant. Basically, the acoustic intensity can be written in the form of a scaling law and the constants can be determined experimentally.

The form of the scaling law for the acoustic intensity from the interaction of turbulence with a single shock derived from equation (2-2-63) is

$$I_{sound} = A_o F(M_J) \left[\left(\frac{\rho_J}{\rho_a} \right)^{0.5} \left(\frac{U_J}{C_a} \right)^{1.0} \right] \overline{\left(\frac{u_{1r}}{U_n} \right)^2} \qquad (2\text{-}2\text{-}64)$$

where A_o = constant, and $F(M_J)$ is some function of M_J.

The reason for writing the scaling law in the form of $\left(\frac{\rho_J}{\rho_a}\right)\left(\frac{U_J}{C_a}\right)^2$ instead of $\left[\left(\frac{\rho_J}{\rho_a}\right)\left(\frac{U_J}{C_a}\right)^2 - 1\right]$ is because both forms are equivalent, and it is more convenient to use the form as in equation (2-2-64).

It must be noted that equation (2-2-64) gives the acoustic intensity from the turbulence interaction of a single shock. To calculate the total acoustic power of the supersonic jet, it is necessary to know the acoustic intensities from the interaction of turbulence with the succeeding shocks in the system of shocks in the supersonic jet. The total acoustic power is then obtained by integrating the contribution of the acoustic intensity from the interaction of turbulence with each shock in the supersonic region. This is done by first calculating the strength of the shocks in the supersonic region, and Part 3 is devoted to such calculations.

Part 3

2.3 Oblique Shock in a Supersonic Jet

The treatment of the oblique shocks in supersonic jets is divided into two sections. Section A is mainly on overexpanded jets where an oblique chock is formed immediately near the exit of the nozzle; and section B is for the underexpanded jets where, instead of a shock, an expansion fan is formed at the nozzle exit. Evidently some internal shock waves cannot be avoided even when the jet is operating under perfectly expanded conditions due to the presence of the shear layer. Therefore, in the present analysis, perfectly expanded jets are treated under the same category as the overexpanded jets.

A. Overexpanded Supersonic Jets

A schematic diagram of the shock cells of an overexpanded jet is given in Fig. 3. For simplicity the non-simple regions and viscous effects are ignored and the analysis is confined to one-half of the cross-section of the jet, since the cross-section is symmetrical about the axis of the jet. Two conditions for the formation of the shock cells must be satisfied:

1) The flow must be parallel to the jet axis inside the shock cells as demanded by the conservations laws;
2) The static pressure outside the shock cells must match the ambient pressure, P_a.

In the first shock, S_1:

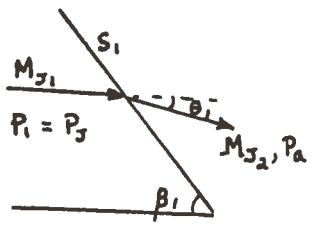

$M_{J1} = M_J$

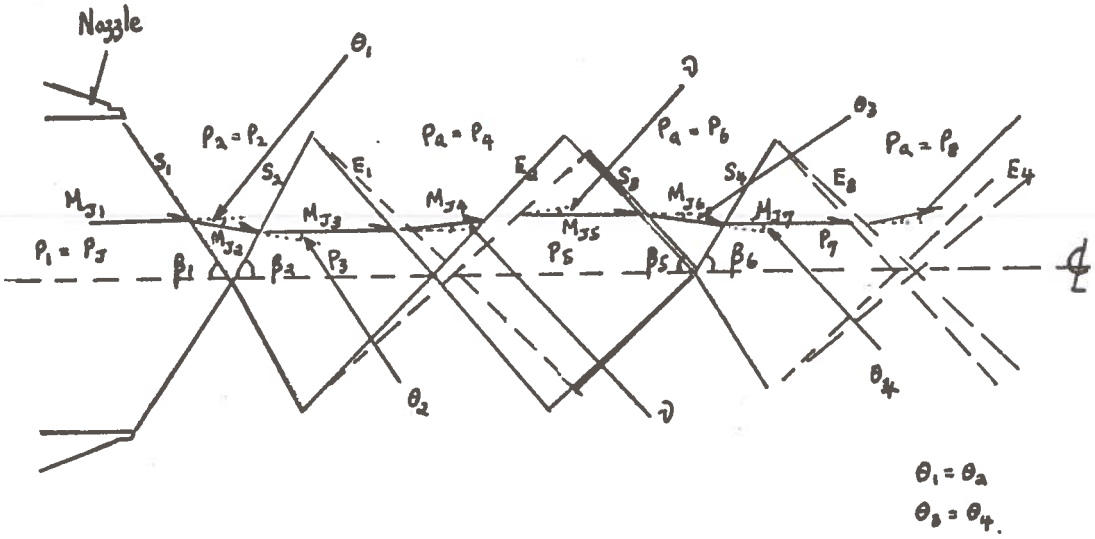

Figure 3: Schematic sketch of an overexpanded supersonic jet showing the shock structures.

$$\frac{P_a - P_J}{P_a} = \frac{2\gamma}{\gamma+1}\left(M_{n_1}^2 - 1\right)$$

$$M_{n_1} = \left\{1 + \frac{\gamma+1}{2\gamma}\left(1 - \frac{P_J}{P_a}\right)\right\}^{1/2} \qquad (2\text{-}3\text{-}1)$$

For $\frac{P_J}{P_a} \simeq 1$

$$M_{n_1} = \left\{1 + \frac{\gamma+1}{4\gamma}\left(1 - \frac{P_J}{P_a}\right)\right\} \qquad (2\text{-}3\text{-}2)$$

Also

$$M_{J_2}^2 \sin^2(\beta_1 - \theta_1) = \frac{1 + \frac{\gamma-1}{2} M_{J_1}^2 \sin^2\beta_1}{\gamma M_{J_1}^2 \sin^2\beta_1 - \frac{\gamma-1}{2}} \qquad (2\text{-}3\text{-}3)$$

$$= \frac{1 + \frac{\gamma-1}{2} M_{n_1}^2}{\gamma M_{n_1}^2 - \frac{\gamma-1}{2}} \qquad (2\text{-}3\text{-}4)$$

$$\tan\theta_1 = \frac{2\cot\beta_1 (M_{n_1}^2 - 1)}{M_{J_1}^2 (\gamma + \cos 2\beta_1) + 2} \qquad (2\text{-}3\text{-}5)$$

where

$$\sin \beta_1 = \frac{M_{n_1}}{M_{J_1}} = \frac{\left\{1 + \frac{\gamma+1}{4\gamma}\left(1 - \frac{P_J}{P_a}\right)\right\}}{M_{J_1}} \qquad (2\text{-}3\text{-}6)$$

for $P_J \simeq P_a$.

Hence, from the above equations, M_{n1}, β_1, θ_1, and M_{J2} could be calculated.

For the second shock, S_2:

$$\tan \theta_1 = \frac{2 \cot \beta_2 \left(M_{n_2}^2 - 1\right)}{M_{J_2}^2 \left\{\gamma + \cos 2(\beta_2 + \theta_1)\right\} + 2} \qquad (2\text{-}3\text{-}7)$$

$$M_{n_2} = M_{J_2} \sin (\beta_2 + \theta_1) \qquad (2\text{-}3\text{-}8)$$

$$\frac{P_3 - P_a}{P_3} = \frac{2\gamma}{\gamma+1}\left(M_{n_2}^2 - 1\right) \qquad (2\text{-}3\text{-}9)$$

Since θ_1 and M_{J2} are known from the above calculations, β_2 can be calculated from equation (2-3-7). Therefore, M_{n2} is known from equation (2-3-8) and P_3 from equation (2-3-9).

Similarly,

$$M_{J_3}^2 \sin^2\beta_2 = \frac{1 + \frac{\gamma-1}{2} M_{J_2}^2 \sin^2(\beta_2 + \theta_1)}{\gamma M_{J_2}^2 \sin^2(\beta_2 + \theta_1) - \frac{\gamma-1}{2}}$$

$$= \frac{1 + \frac{\gamma-1}{2} M_{n_2}^2}{\gamma M_{n_2}^2 - \frac{\gamma-1}{2}} \qquad (2\text{-}3\text{-}10)$$

Therefore, M_{J3} can also be calculated from the above equation.

The pressure P_3 is greater than P_a and the flow undergoes an isentropic expansion through a Prandtl-Meyer expansion fan.

For the first P-M expansion fan, E_1:

$$\frac{P_3}{P_a} = \frac{\left(1 + \frac{\gamma-1}{2} M_{J4}^2\right)^{\gamma/\gamma-1}}{\left(1 + \frac{\gamma-1}{2} M_{J3}^2\right)^{\gamma/\gamma-1}} \qquad (2\text{-}3\text{-}11)$$

and M_{J4} is known from the above equation. The turning angle of the flow through E_1 is given by the P-M relation

$$\nu(M) = \nu(M_{J_4}) - \nu(M_{J_3}) \qquad (2\text{-}3\text{-}12)$$

where

$$\nu(M_{J4}) = \sqrt{\frac{\gamma+1}{\gamma-1}} \tan^{-1}\sqrt{\frac{\gamma-1}{\gamma+1}(M_{J4}^2 - 1)} - \tan^{-1}\sqrt{M_{J4}^2 - 1} \qquad (2\text{-}3\text{-}13)$$

$$\nu(M_{J_3}) = \sqrt{\frac{\gamma+1}{\gamma-1}}\tan^{-1}\sqrt{\frac{\gamma-1}{\gamma+1}\left(M_{J_3}^2-1\right)} - \tan^{-1}\sqrt{M_{J_3}^2-1} \qquad (2\text{-}3\text{-}14)$$

On reaching the second P-M expansion fan, the flow is further turned by another angle $\nu(M)$ so that the flow is parallel to the jet axis inside the shock cell.

For the second P-M expansion fan, E_2: the Mach number of the flow, M_{J5}, corresponding to the second turning is given by the P-M relation with

$$\nu(M_{J_5}) = \nu(M_{J_3}) + 2\nu(M) \qquad (2\text{-}3\text{-}15)$$

From P-M tables, M_{J5} can be calculated. Furthermore, the pressure P_5 is obtained from the isentropic relation

$$\frac{P_5}{P_a} = \left\{\frac{1+\frac{\gamma-1}{2}M_{J4}^2}{1+\frac{\gamma-1}{2}M_{J5}^2}\right\}^{\gamma/\gamma-1} \qquad (2\text{-}3\text{-}16)$$

In the third shock, S_3:

$$\frac{P_a - P_5}{P_a} = \frac{2\gamma}{\gamma+1}\left\{M_{J_5}^2 \sin^2\beta_5 - 1\right\}$$

$$= \frac{2\gamma}{\gamma+1}\left\{M_{n_3}^2 - 1\right\} \qquad (2\text{-}3\text{-}17)$$

$$M_{n_3} = M_{J_5} \sin\beta_5 \qquad (2\text{-}3\text{-}18)$$

$$\tan\theta_3 = \frac{2\cot\beta_5 (M_{n_3}^2 - 1)}{M_{J_5}^2(\gamma + \cos 2\beta_5) + 2} \qquad (2\text{-}3\text{-}19)$$

From the above equations, M_{n3}, β_5 and θ_3 are known. Also,

$$M_{J_6}^2 \sin^2(\beta_5 - \theta_3) = \frac{1 + \frac{\gamma-1}{2} M_{J_5}^2 \sin^2\beta_5}{\gamma M_{J_5}^2 \sin^2\beta_5}$$

$$= \frac{1 + \frac{\gamma-1}{2} M_{n_3}^2}{\gamma M_{n_3}^2 - \frac{\gamma-1}{2}} \qquad (2\text{-}3\text{-}20)$$

Therefore, M_{J6} is also known.

In the fourth shock, S_4:

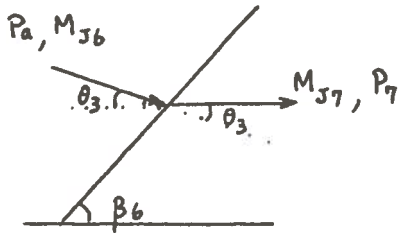

$$\tan\theta_3 = \frac{2\cot(\beta_6+\theta_3)(M_{n_4}^2-1)}{M_{J_6}^2\{\gamma+\cos 2(\beta_6+\theta_3)\}+2} \qquad (2\text{-}3\text{-}21)$$

where $$M_{n_4} = M_{J_6}\sin(\beta_6+\theta_3) \qquad (2\text{-}3\text{-}22)$$

Since θ_3 and M_{J6} are known and M_{n4} is related to Sin $(\beta_6 + \theta_3)$ in equation (2-3-22), β_6 can be obtained and hence M_{n4} can also be calculated.

In principle, the analysis can be extended to any number of shock cells. In this analysis, it is sufficient to consider only four shock cells.

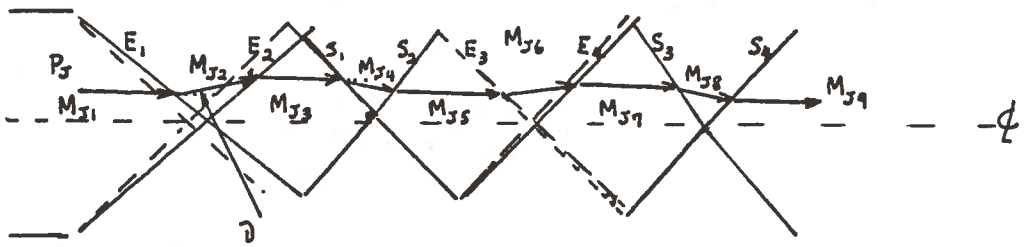

Figure 4: Schematic sketch of an underexpanded supersonic jet showing the shock structures.

B. Underexpanded Supersonic Jets

A schematic sketch of an underexpanded supersonic jet is illustrated in Fig. 4. In the underexpanded jet, a P-M expansion fan is formed at the exit of the nozzle:

$$\frac{P_J}{P_a} = \left\{ \frac{1 + \frac{\gamma-1}{2} M_{J_2}^2}{1 + \frac{\gamma-1}{2} M_{J_1}^2} \right\}^{\gamma/\gamma-1} \qquad (2\text{-}3\text{-}23)$$

The turning angle of the flow is determined by the P-M relation

$$\nu(M) = \nu(M_{J_2}) - \nu(M_{J_1}) \qquad (2\text{-}3\text{-}24)$$

where

$$\nu(M_{J_2}) = \sqrt{\frac{\gamma+1}{\gamma-1}} \tan^{-1} \sqrt{\frac{\gamma-1}{\gamma+1}\left(M_{J_2}^2 - 1\right)} - \tan^{-1} \sqrt{M_{J_2}^2 - 1} \qquad (2\text{-}3\text{-}25)$$

$$\nu(M_{J_1}) = \sqrt{\frac{\gamma+1}{\gamma-1}} \tan^{-1} \sqrt{\frac{\gamma-1}{\gamma+1}\left(M_{J_1}^2 - 1\right)} - \tan^{-1} \sqrt{M_{J_1}^2 - 1} \qquad (2\text{-}3\text{-}26)$$

On reaching the second P-M expansion fan, the flow is further turned by another angle $\nu(M)$ so that the flow is parallel to the jet axis inside the shock cell. The rest of the analysis is the same as in the over-

expanded supersonic jet.

Length of Shock Cells and Total Acoustic Power

The total acoustic power is obtained by integrating the intensity over the length of the system of shocks. Price has given the following relation for the length of the shock cells:

$$\frac{s}{d} = 1{\cdot}2\left\{\frac{P_J}{P_a}\left(1+\frac{\gamma-1}{2}M_J^2\right)^{\gamma/\gamma-1} - 2{\cdot}39\right\}^{0{\cdot}35}$$

and

$$L_s^* = 1{\cdot}2n\left\{\frac{P_J}{P_a}\left(1+\frac{\gamma-1}{2}M_J^2\right)^{\gamma/\gamma-1} - 2{\cdot}39\right\}^{0{\cdot}35}$$

$$= 1{\cdot}2n\left\{\left(\frac{\rho_J}{\rho_a}\right)\left(\frac{B_0}{M_J^2}\right)\left(\frac{U_J^2}{Ca^2}\right)\left(1+\frac{\gamma-1}{2}M_J^2\right)^{\gamma/\gamma-1} - 2{\cdot}39\right\}^{0{\cdot}35}$$

The noise sources would appear to be concentrated around the shock-tips where the conical surfaces of the oblique shock interact with the vorticity or turbulence in the shear layer. If the noise sources due to the interaction of the shocks are uncorrelated, the acoustic intensities combine linearly.

III. DERIVATION OF A SCALING LAW FOR THE TOTAL ACOUSTIC POWER FROM CIRCULAR SUPERSONIC JETS BASED ON THE THEORY OF SHOCK-TURBULENCE INTERACTION

Total Acoustic Power

The calculation of the strengths of the first four shocks in the overexpanded $\frac{P_J}{P_a} = \frac{17}{23}$ and the underexpanded jet $\frac{P_J}{P_a} = \frac{29}{23}$ for $M_J = 2.74$ is given in Appendix B. The interaction terms represented by the average transfer function $\overline{S_p^{v2}}$ is dependent on the strength of the shocks and the interaction terms for each of the four shocks is plotted against the average location of the shocks. The resulting distribution of the interaction terms $\overline{S_p^{v2}}$ given in Appendix B for the overexpanded and underexpanded jets suggests the interaction terms can be approximated by an inverse linear function. The interaction terms for the succeeding shocks can be expressed as

$$\left[\overline{S_p^{v2}}\right]_{2^{nd}\ shock} = \left[\overline{S_p^{v2}}\right]_{1^{st}\ shock} \left[\frac{x}{d}\right]^{-1} \qquad (3\text{-}1)$$

where $[\frac{x}{d}]$ is given by the location of the mean radius of the second shock. Similarly for the third and the succeeding shocks in the supersonic region, the interaction terms can be represented by equation (3-1).

The first approximation is to assume the mean square vorticity fluctuation to be constant along the axial distance, but experimental work by Goldberg[16] suggests that the mean square vorticity fluctuation is dependent on the upstream history and is increasing along the axial axial distance. Physically it means that as the eddies in the shear

layer are breaking up into smaller eddies, the number of eddies per unit volume of turbulence also increases and hence the mean square vorticity fluctuation. For simplicity, assume the distribution of the mean square vorticity fluctuation along the axial distance to be

$$\overline{\left(\frac{u_{lv}}{u_n}\right)^2}_x = \overline{\left(\frac{u_{lv}}{u_n}\right)^2}_{x=0} x^a \qquad (3\text{-}2)$$

so that the mean square vorticity fluctuation is constant along the axial distance when a = 0 and is linearly proportional to the axial distance when a = 1. This assumption does not violate the isotropic turbulence assumption on which the average transfer functions are evaluated.

Further assume that the sources of noise generation due to turbulence interaction with each of the shocks in the supersonic jet are uncorrelated; then the acoustic power output per unit length of the jet can be expressed as

$$I_x = A_0 F(M_J) \left[\left(\frac{\rho_J}{\rho_a}\right)^{0.5} \left(\frac{u_J}{C_a}\right)^{1.0}\right] \overline{\left(\frac{u_{lv}}{u_n}\right)^2}_{x=0} x^{a-1} \qquad (3\text{-}3)$$

and the total acoustic power output (PWL) of the jet is

$$PWL = \int_0^{L_s} I_x dx = A_o F(M_J) \left[\left(\frac{\rho_J}{\rho_a}\right)^{0.5} \left(\frac{u_J}{C_a}\right)^{1.0}\right] \left(\frac{\overline{u_{IV}}}{u_n}\right)^2_{x=0} \frac{L_s}{a}^a$$

$$= \frac{1.2 n A_o}{a} F(M_J) \left[\left(\frac{\rho_J}{\rho_a}\right)^{0.5} \left(\frac{u_J}{C_a}\right)^{1.0}\right] \left[\left(\frac{\rho_J}{\rho_a}\right) \left(\frac{u_J}{C_a}\right)^2 \times \right.$$

$$\left. \times \left(1 + \frac{\gamma-1}{2} M_J^2\right)^{\gamma/\gamma-1} - 2.39 \right]^{0.35} \left(\frac{\overline{u_{IV}}}{u_n}\right)^2_{x=0} \qquad (3\text{-}4)$$

Therefore, the form of a scaling law derived for the PWL for circular jets from the above expression is

$$PWL = B_o G(M_J) \left[\left(\frac{\rho_J}{\rho_a}\right)^{0.5+0.35a} \left(\frac{u_J}{C_a}\right)^{1.0+0.7a}\right] \left(\frac{\overline{u_{IV}}}{u_n}\right)^2_{x=0} \qquad (3\text{-}5)$$

B_o is some constant, and $G(M_J)$ is some function of M_J. There is no data available on the direct correlation of the mean square vorticity fluctuation with the jet flow parameters. Theoretically it is possible to measure the mean square vorticity fluctuation using hot wire probes and measure the voltage output as the flow parameters are changed, and

an approximate relation for the variation of the mean square vorticity fluctuation with flow parameters can be obtained. However, it must be cautioned that such a relation is not universal and is only approximate for the individual nozzle. From dimensional analysis, the mean square vorticity fluctuation is going to be dependent on the Reynolds number Re, the Reynolds stresses $\rho_i v_i v_j$, the local velocity profile, the upstream history and other factors. But essentially, the Reynolds stresses $\rho_i v_i v_j$ is the most important consideration since it represents the variable rates of momentum flux across surfaces fixed in the fluctuating fluid flow. It must be realized that the turbulence or vorticity field in the shear layer in the supersonic jet is assumed to be isotropic but not necessarily homogeneous. The following approximation for the mean square vorticity fluctuation is suggested:

$$\overline{\left(\frac{u_{lv}}{u_n}\right)^2}_{x=0} \propto \text{momentum flux} \propto u_J^2 \qquad (3\text{-}6)$$

Basically, what equation (3-6) says is that the <u>percentage</u> of vorticity fluctuation is constant, or

$$\frac{\overline{\left(\frac{u_{lv}}{u_n}\right)^2}_{x=0}}{\rho_a u_J^2} = \text{constant} \qquad (3\text{-}7)$$

Therefore, the form of the scaling law for the acoustic power output from the circular supersonic jet is

$$PWL = \text{constant} \times G(M_J) \left(\frac{\rho_J}{\rho_a}\right)^{0.5+0.35a} \left(\frac{u_J}{C_a}\right)^{3.0+0.7a} \qquad (3\text{-}8)$$

IV. EXPERIMENTAL FACILITIES AND TECHNIQUE

4.1 Shock Tunnel

A shock tunnel is used to create the cold and hot jets in this investigation. By first changing the driver, driven pressures and molecular weights of the gas, a wide range of stagnation pressures and temperatures could be achieved. Argon (γ = 1.67) is chosen as the test gas.

The shock tunnel consists essentially of a high pressure section (18 feet long) and a low pressure section (21 feet long) separated by a thin diaphragm. On the diaphragm a diagonal groove is cut so that when the diaphragm bursts open the petals of the diaphragm fold neatly into the adapted section of the low pressure chamber giving a constant cross-sectional area over the entire length of the shock tunnel. The depth of the groove on the diaphragm is calibrated so that the diaphragm will break consistently when the same driver and driven pressures are used. With the shock tunnel the test time is very short and is of the order of 10-15 milliseconds. The apparent advantages of using such short test time are that the nozzles can simply be heat-sink nozzles and there is no necessity of an anechoic chamber. Two methods are used to test the consistency of each run as regards to the stagnation temperature and pressure. One method is to keep the shock speed constant so that the stagnation temperature and pressure, T_s and P_s, are constant; the other method is to keep a microphone at some fixed distance from the nozzle exit so that the variation of the SPL of the microphone from run to run gives the inconsistency of each run. A detailed discussion of the

consistency of reproducing each run using this technique is given by Louis et al.[17]

As the diaphragm between the driver and driven chambers is ruptured, a shock wave is created which propagates in the low pressure section of the shock tunnel. The incident shock on reflecting from the nozzle side of the tunnel leaves behind a region of high stagnation pressure and temperature. This condition remains constant until the interface or the expansion fan catches up with the reflected shock. A longer steady-state test time is available by using a "tailored-interface" technique. A detailed description of the technique is given in Refs. 8 and 18.

Figure 5 shows the time distance history in the shock tunnel. The incident shock speed is measured by means of three Kistler pressure transducers (rise time of about 10 microseconds) mounted 3 feet apart on the shock tube, as indicated in Fig. 5. Knowing the time interval for the incident shock to travel 3 feet (distance between two Kistler pressure transducers), the shock Mach number, M_s, is easily obtained. The relation for the stagnation temperature and pressure is given by

$$\frac{T_5}{T_1} = \frac{\left[2(\gamma-1)M_s^2 + (3-\gamma)\right]\left[(3\gamma-1)M_s^2 - 2(\gamma-1)\right]}{(\gamma+1)^2 M_s^2} \qquad (4\text{-}1\text{-}1)$$

$$\frac{P_5}{P_1} = \left[\frac{2\gamma M_s^2 - (\gamma-1)}{\gamma+1}\right]\left[\frac{(3\gamma-1)M_s^2 - 2(\gamma-1)}{(\gamma-1)M_s^2 + 2}\right] \qquad (4\text{-}1\text{-}2)$$

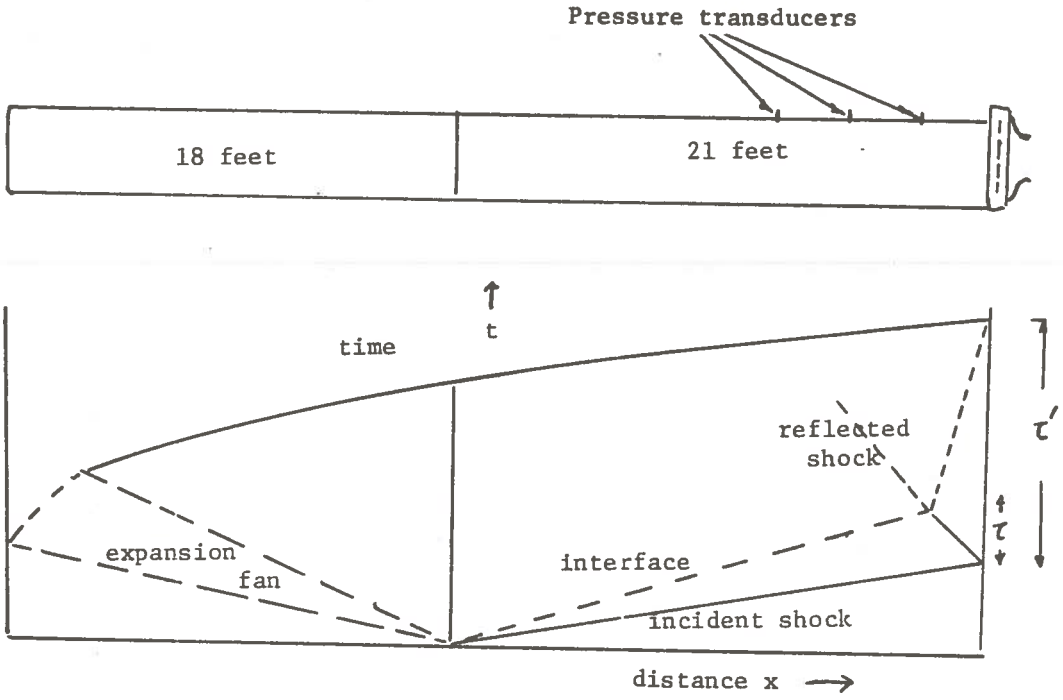

τ - test time without interface-tailored technique

τ' - test time with interface-tailored technique

Figure 5: Time, Distance, History in Shock Tunnel.

P_1 is the pressure in the driven section and it is accurately monitored by a mercury manometer. Thus, knowing P_1 and T_1 (ambient temperature) and the shock Mach number M_s, P_5 and T_5 are obtained.

4.2 Circular Supersonic Nozzles and Rectangular Nozzles

Three circular supersonic nozzles corresponding to exit Mach numbers M_J of 2.74, 2.3 and 1.8 ($\gamma = 1.67$) are used in the experiments. These are heat sink nozzles made of aluminum material. The nozzles are computer designed to give uniform parallel flow at the nozzle exit, and they have identical throat diameters (d = 0.876 in.) so that they give identical mass flux under identical operating conditions.

The rectangular nozzle is made of glass reinforced epoxy. It is designed in two parts, a convergent part which could be easily adapted to the shock tube, and a divergent part designed to provide a source flow. It has the same throat area as the circular or axisymmetric nozzles, and a 3% drop in theoretical propulsive efficiency is associated with this nozzle.

The circular nozzles and the rectangular nozzle are shown in Fig. 6.

4.3 Microphones and Ampex Tape Recorder

With the help of five B&K 1/8-in. condenser microphones, the data are recorded on a 14-channel Ampex FR 1900 multiband instrument tape recorder. At the beginning of each set of runs, the microphones are calibrated with a B&K 4220 piston phone which has a reference of 124 decibels at 250 Hertz. Another method of calibration also used is to record the response of each microphone to the reference SPL of 124 db from the piston on the tape recorder. The signals are then digitalized and reduced by computer programs written specifically for calculating the RMS. The two methods of

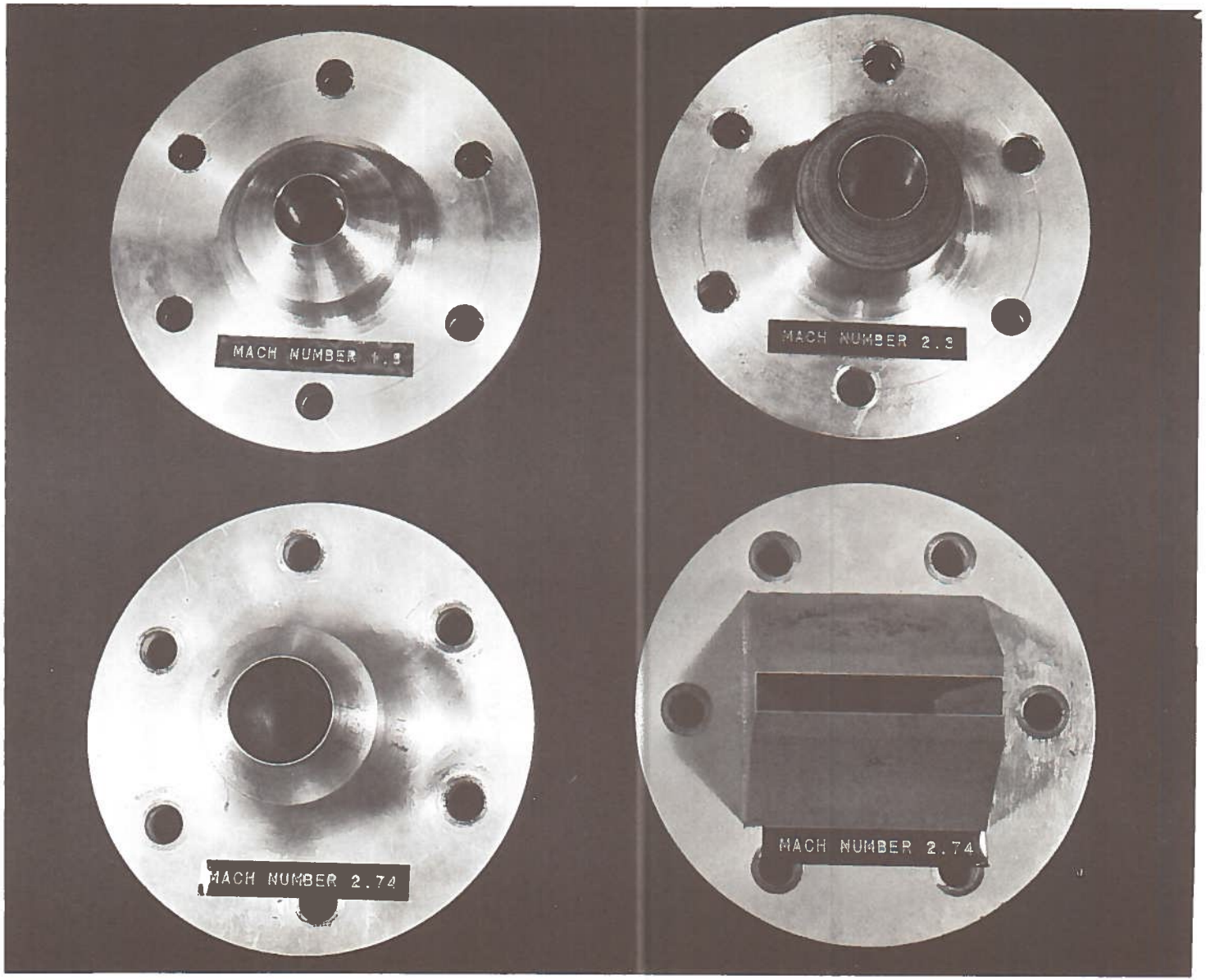

Figure 6: Circular Nozzles and Rectangular Nozzle.

calibration give the sensitivities of the microphones to an agreement within a few percent. These B&K microphones have a frequency range from 30 Hz to 140 KHz and a dynamic range up to 184 lb. re. 0.0002 bars. Figure 7 shows part of the experimental setup.

4.4 Data Acquisition

Since the jet is axisymmetric, measurement is made on one plane only. Measurements are made by placing the microphones six inches apart starting from the lip of the nozzle to about 43.0 diameters downstream along a line parallel to the jet axis and at a radial distance of 23.5 diameters. With duration of test time in the order of milliseconds, it is necessary to record at the fastest speed (120 inches/sec.). The signal from the first Kistler pressure transducer is connected to a charge amplifier which converts the high-impedance signal to a voltage signal, which is then used to trigger the oscilloscope and also is recorded in one of the channels used for the gating signal. The gating signal is used to control the start of the analog-to-digital conversion of the signals of the test runs so that only the actual data are digitalized.

4.5 Data Reduction

The conventional methods used for analog signal analysis are not suitable because the test time is so short. Hence, the method chosen for data analysis is digital processing. The signal is first reduced on an A/D (analog-to-digital) converter using the Adage AGT-30 to binary values, and is stored in the form of blocks, each block containing 1024 points (2^8) on a seven-track digital tape. A subroutine converts these binary values into two one-dimensional arrays: voltage and time. The sampling frequency of 200 KHz for the A/D converter, supplied by a

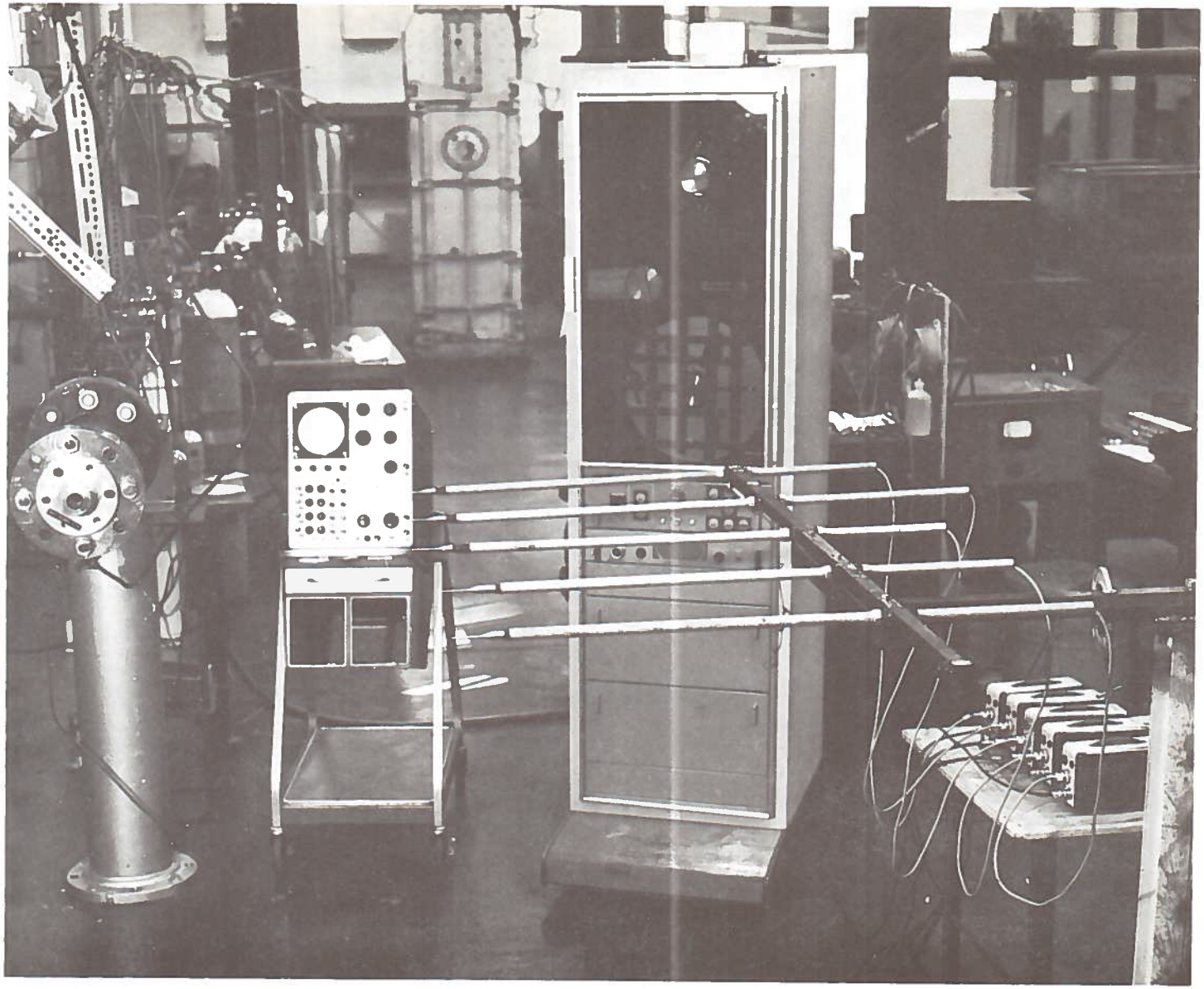

Figure 7: Experimental Setup and Facilities.

direct record channel (which is also the control track for the tape recorder), is reduced by a factor of 64 when the signal is played back at 1-7/8 inch/sec. In terms of real test time, the sampling interval is 5 μs.

A detailed description of the computer program for the A/D conversion is given in Ref. 19. The RMS value of each digitalized signal is obtained by means of computer programs in conjunction with the IBM 360/65 operating system. In the computer program the interval of the sampling block for the calculation of the RMS is 5.12 msec. in real test time, and the starting of the sampling is delayed by different intervals of time from the start of the digitalized signal so that a complete Time-RMS history of the response of each microphone is obtained. This technique is particularly useful for determining when the flow has reached steady state and the duration of the steady-state flow condition. The Time-RMS history of the response of a single microphone in a typical run is given in Table 1. The reason why the steady state is reached after 8.0 msec. instead of 2-3 msec. is because the gating or trigger signal is from a pressure transducer located 9 feet upstream of the nozzle exit and thus the gating signal is about 5 msec. early at the start of the A/D conversion. This method is helpful as it will eliminate any extraneous noise in the initial phase of the gating of the signal in the A/D conversion process.

4.6 Sound Power Level (SPL)

Simcox[20] has suggested that in order to compare the local SPL for jets having different K.E and jet Mach numbers, a normalized SPL based on the mass flow rate should be used:

TABLE 1. Time-RMS History of the Response of a Single Microphone in a Typical Run.

Delay Time from Start of Gating Signal (msec)	5.6	6.35	7.10	7.85	8.60	9.35	10.10	10.75	11.50	12.25	13.00
RMS of Signal	0.1072	0.1096	0.1125	0.0804	0.0698	0.0668	0.0675	0.0680	0.0687	0.0690	0.0695

STEADY STATE

$$SPL_c = SPL - 10 \log A_T \qquad (4\text{-}6\text{-}1)$$

where A_T = throat area.

Since all the nozzles are designed with the same throat area A_T, no correction is necessary when comparing the local SPL.

To perform the calculation of the total acoustic power PWL, integration is performed on a cylindrical surface of radius = 23.5 jet diameters and running co-axial to the jet and extending as far as 43.0 jet diameters downstream from the nozzle exit. The conventional way of calculating the total acoustic power output is to integrate the sound pressure level over a hemispherical surface of radius R, which is given by

$$PWL = \frac{2\pi R^2}{\rho_a C_a} \int_0^{2\pi} \overline{P^2} \sin\theta \, d\theta$$

Because of the location of our present facilities, the method of calculating the total sound power level by integrating the SPL over a cylindrical surface is adopted.

The total acoustic power is

$$PWL = \frac{1}{\rho_a C_a} \int_0^{L} \overline{P_n^2} \, 2\pi R \, dx$$

The errors associated with this method of calculating the total acoustic power amount to about ±0.40 lb. and are known as fixed errors. Since

this method is used consistently throughout the entire experiment, a direct comparison of the results should be valid.

4.7 Calculations of the Jet Density and Jet Velocity

The density of the jet ρ_J is determined from the perfect gas law relation

$$\rho_J = \frac{P_J}{RT_J} \tag{4-7-1}$$

and the isentropic equation

$$\frac{P_o}{P_J} = \left(1 + \frac{\gamma-1}{2} M_J^2\right)^{\gamma/\gamma-1} \tag{4-7-2}$$

$$\frac{T_o}{T_J} = \left(1 + \frac{\gamma-1}{2} M_J^2\right)^{\gamma/\gamma-1} \tag{4-7-3}$$

P_o and T_o are the stagnation pressure and temperature conditions of the jet.

The jet velocity U_J is taken at the exit plane of the jet:

$$U_J = M_J \sqrt{\gamma \frac{R}{M} T_J} \tag{4-7-4}$$

The ambient pressure P_a is taken to be standard atmospheric pressure at 80°F which is the normal laboratory temperature, the ambient density

ρ_a is 0.073 lb/ft^3, and the atmospheric sound velocity is taken as 1142 ft/sec. at 80°F.

4.8 Shadowgraphs

Shadowgraphs, shown in Figs. 8 - 12, are taken for the M_J = 2.3 circular jets for temperature conditions corresponding to 4900°R and 1350°R and under different expansion levels: underexpanded, perfectly expanded, and overexpanded. Shadowgraphs for the rectangular and the circular jets for M_J = 2.74 are shown in Patel's[8] and Letty's[21] studies. Since shadowgraphs give the second derivative of the density, waves which appear to be prominent on the shadowgraphs are not necessarily waves which have the highest sound pressure level. Shadowgraphs are taken primarily as an aid in understanding the structures of the jet and the basic noise generating mechanisms.

The experimental setup for taking the shadowgraphs is indicated in Fig. 13. A pressure transducer is located about 8-9 feet downstream from the nozzle exit and centered on the jet axis. The signal from the transducer is connected to a time delay generator and the delayed signal is used to trigger the discharge of a high voltage power source to produce a spark of the duration of 6-10 μsec. The time delay is adjusted so that the spark occurs only after the jet has obtained steady state and the shock bow wave has gone far downstream.

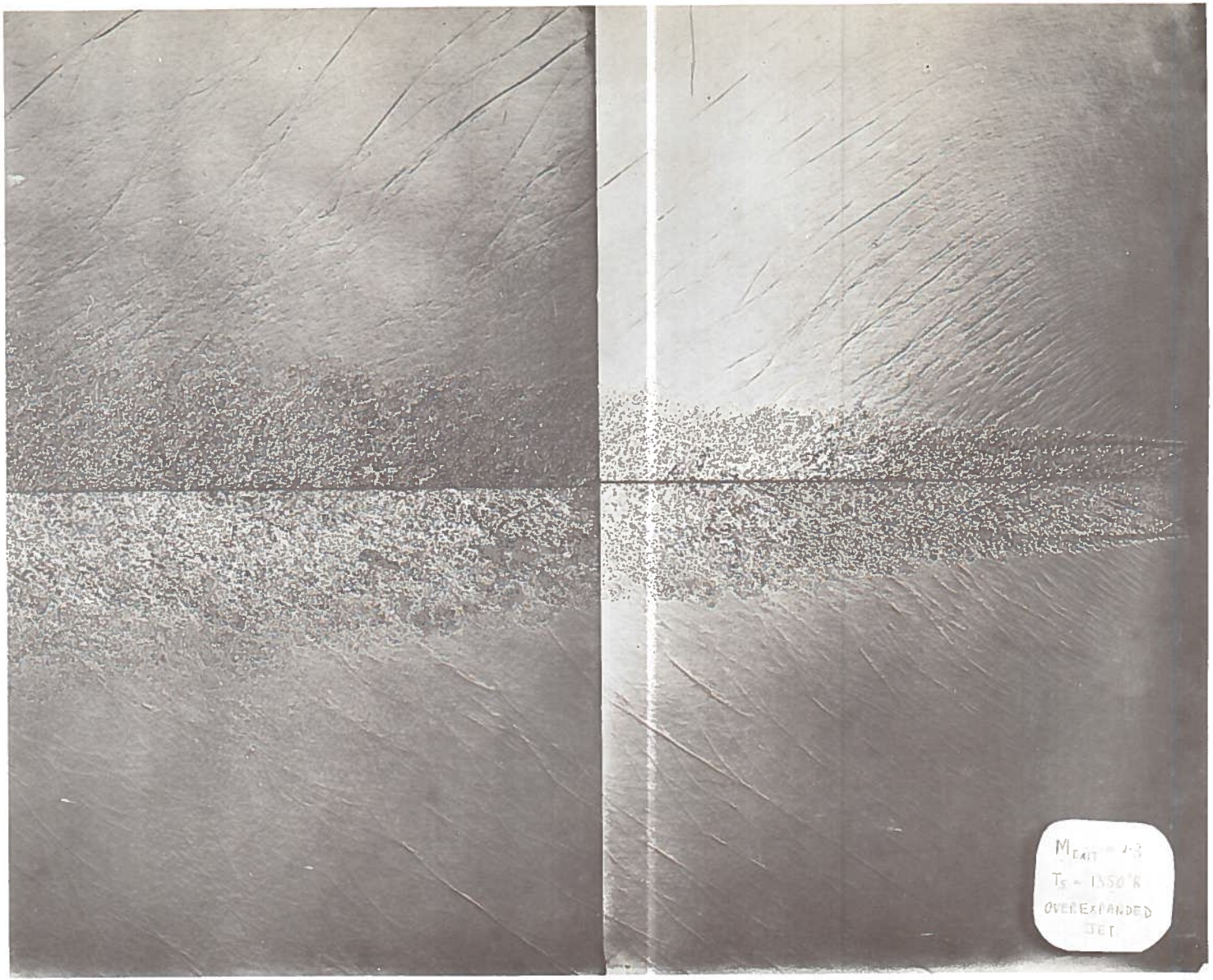

Figure 8: Shadowgraph - overexpanded supersonic jet for jet stagnation temperature of 1350°R.

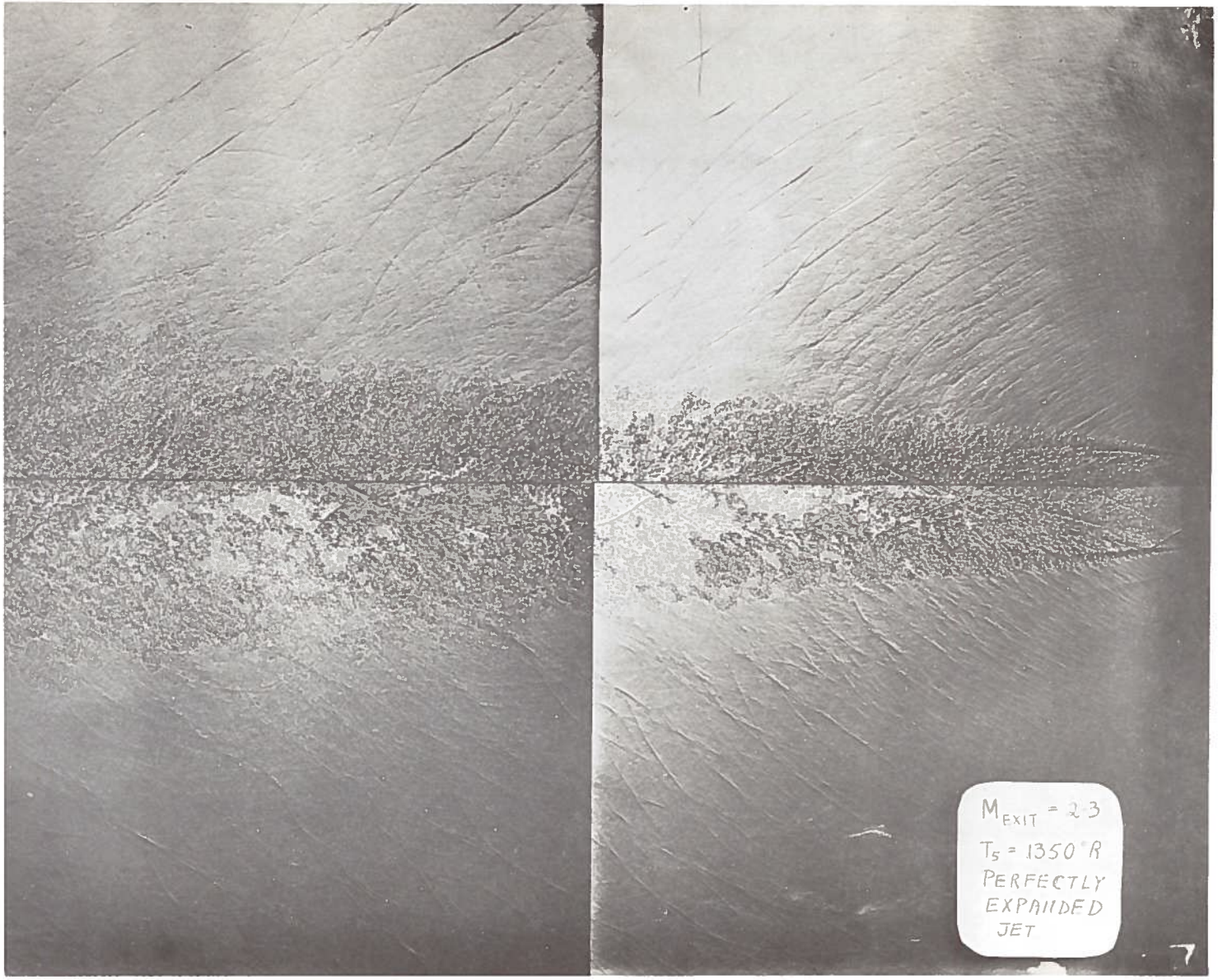

Figure 9: Shadowgraph - perfectly expanded supersonic jet for jet stagnation temperature of 1350°R.

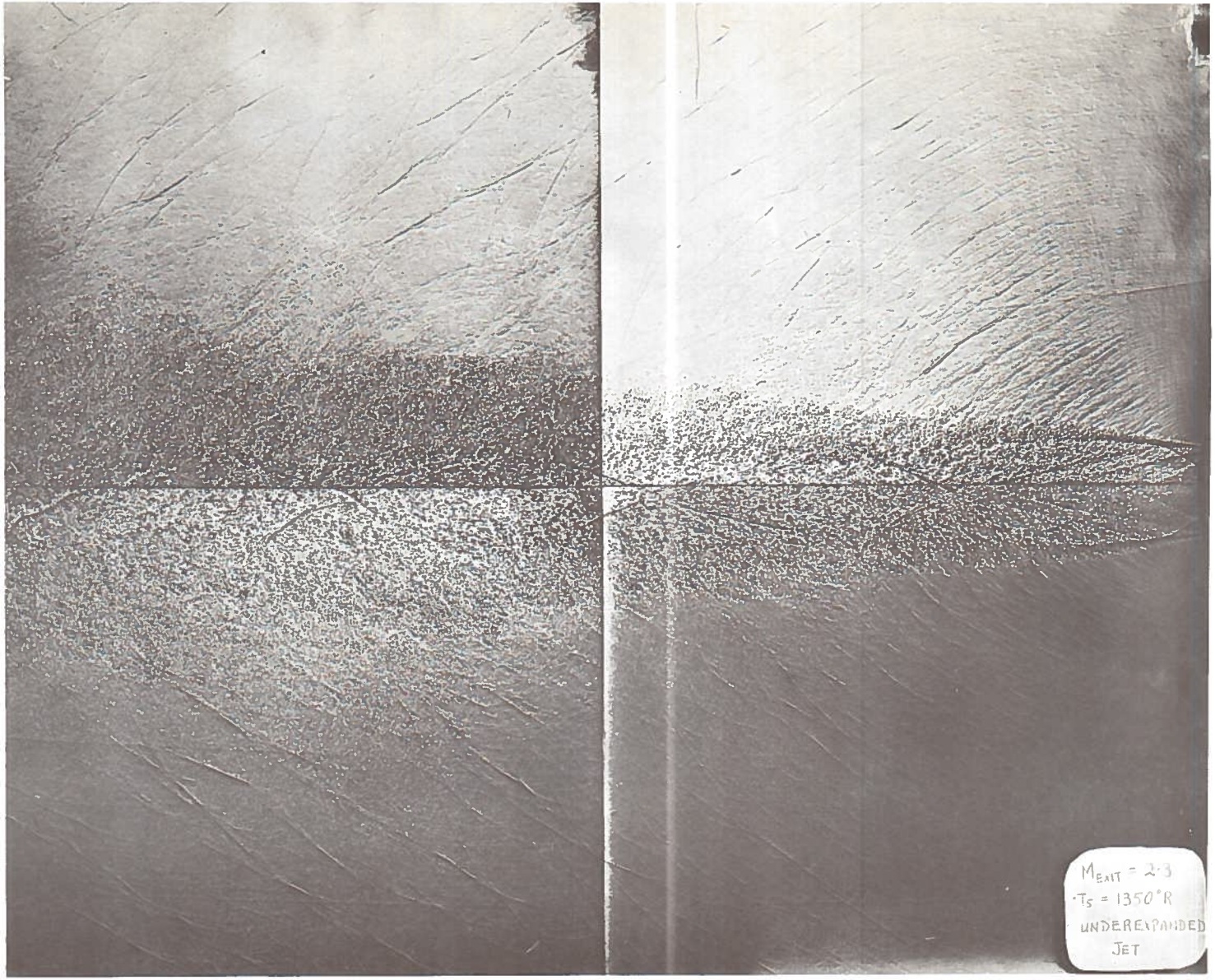

Figure 10: Shadowgraph - underexpanded supersonic jet for jet stagnation temperature of 1350°R.

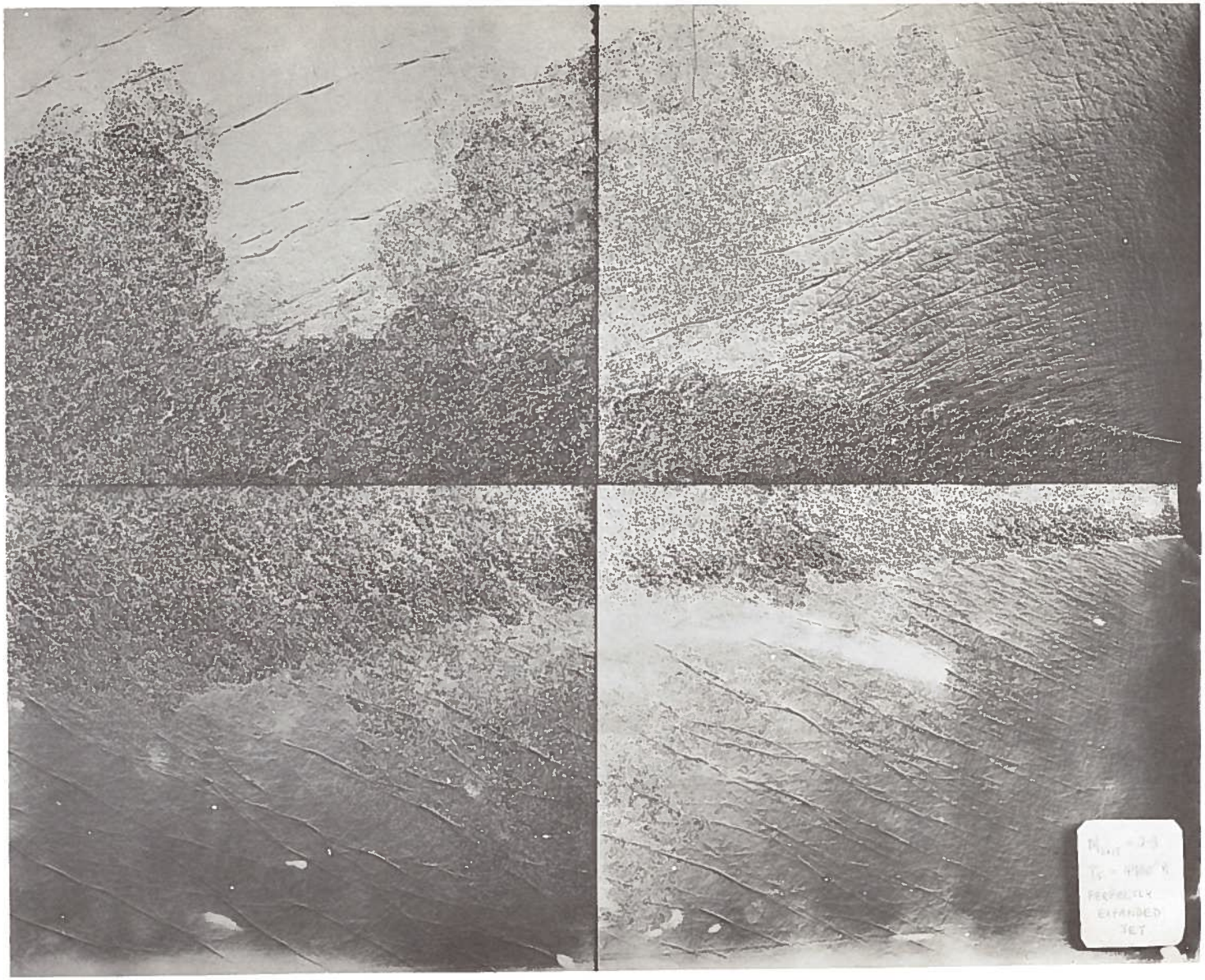

Figure 11: Shadowgraph - perfectly expanded supersonic jet for jet stagnation temperature of 4900°R.

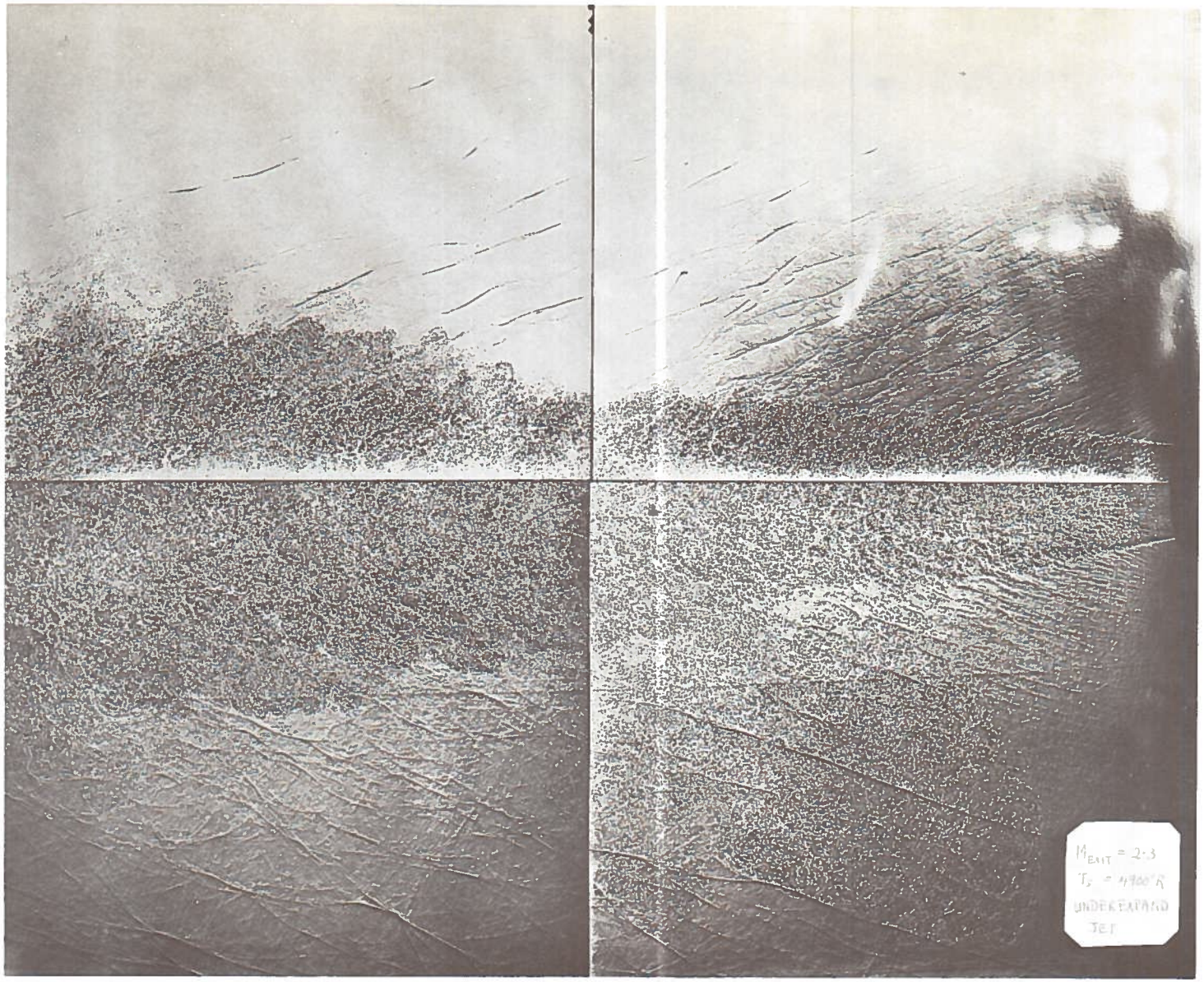

Figure 12: Shadowgraph - underexpanded supersonic jet for jet stagnation temperature of 4900°R.

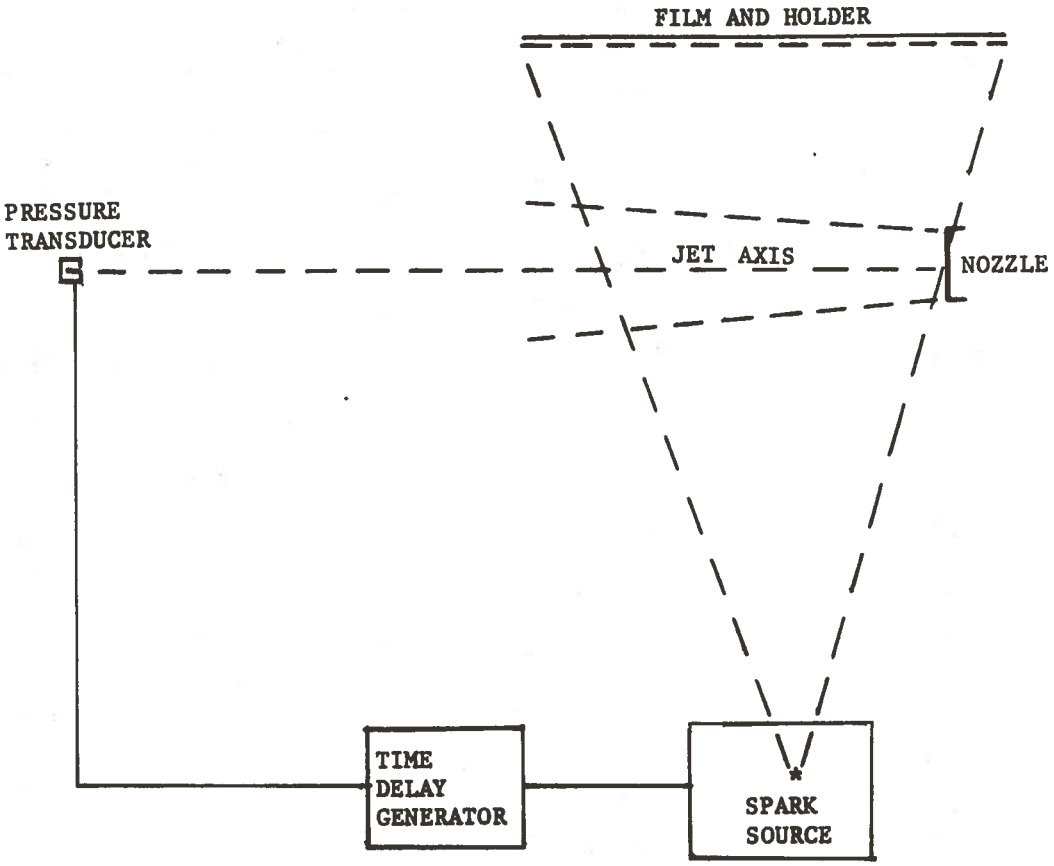

Figure 13: Schematic sketch of setup for taking shadowgraphs.

V. EXPERIMENTAL RESULTS AND ANALYSIS

5.1 Frequency Spectra Analysis of the Mach and Lip Waves Emanating from the Rectangular Nozzle

This analysis is directed to the further understanding of the noise mechanism of the Mach waves. In the turbulent shear layer in the region close to the nozzle, both Mach waves and lip waves seem to be originated from the same sources. There is some possibility that Mach waves may initially start as cylindrical waves which amplify and get scattered by turbulence generated in the shear layer. To study this possibility, two microphones are placed symmetrically in the exit plane of the nozzle and moved from 6 inches to 14 inches along the small axis of the rectangular section. Two more microphones are placed symmetrically in the plane of the jet axis and nozzle small axis. Their locations are moved from 6 inches to 48 inches in the direction of propagation of the Mach waves as obtained from shadowgraphs. Figure 14 gives the schematic display of the microphones with respect to the jet axis and the two regions of interest: the lip wave and the Mach wave regions.

5.1.1 Computational procedure

For each operating point corresponding to a set of stagnation pressure and temperature conditions, a minimum of seven runs are made. Within each run different parts of the data are analyzed for power spectrum. Only 5.12 msec. of data is selected at any given time for spectrum analysis and a minimum of 8-9 samples are taken in each run. A digital computer program has been developed for the analysis of the output signals of the microphones. The signals are stored on a tape in a digitized manner with digitization time of 5 μsec. The length of each data signal is 5.12 msec. which is divided into 8 or 9 subintervals; each group is

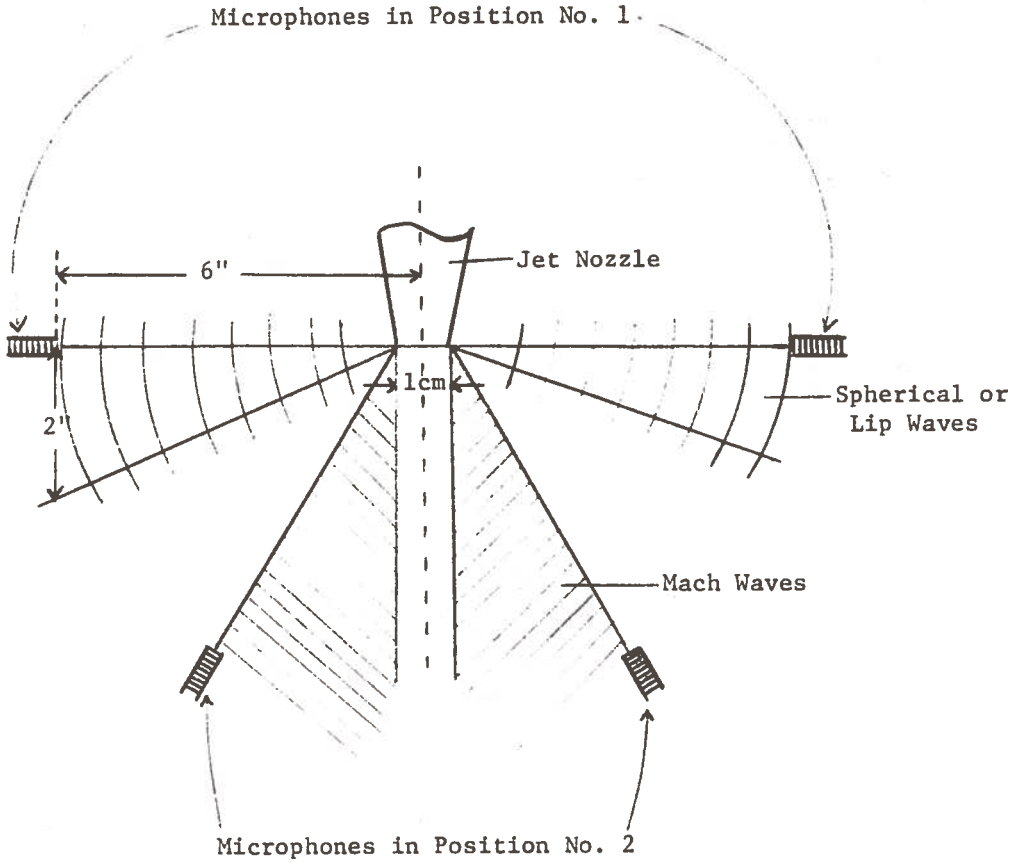

Figure 14: Schematic layout of microphone locations in Mach wave and lip wave regions.

Fourier-analyzed for power spectra, averaged over the total number of signal groups, and cross-correlated with the same output of the other signal coming from the symmetrically positioned microphone.

5.1.2 Flow Steadiness

An average RMS is also computed for each sample. A comparison of the RMS values obtained for the 9 samples of a typical run indicates that the flow has reached a steady state in a time smaller than 2 msec and lasts for a period longer than 10 msec.

Delay from Initial Signal (msec)	RMS Pressure (volt)	Difference from Average (%)
1.1	0.3902	- 0.3
1.6	0.3870	- 1.1
2.1	0.3876	- 0.9
2.6	0.3911	0
3.1	0.3888	- 0.6
3.6	0.3884	- 0.7
4.1	0.3946	+ 0.9
4.6	0.3970	+ 1.5
5.1	0.3966	+ 1.4

5.2 Frequency Spectra of the Mach and Lip Waves

5.2.1 Low Temperature Analysis

The low temperature data are obtained with a stagnation temperature of 1350°R for three expansion levels corresponding to overexpanded, perfectly expanded and underexpanded conditions of the rectangular jet. The statistical observations made on an ensemble of 7 runs for each microphone location indicate:

1) cylindrical waves have well defined peaks: 5.3 KHz for underexpanded, 5.7 KHz for perfectly expanded, and 8.2 KHz for overexpanded conditions;
2) the peaks of the Mach waves are generally higher than the peaks of the cylindrical waves and it appears that the Mach waves' lower spectra have several peaks, also found in the lip wave spectra;
3) close to the nozzle, the spectra show distinct peaks, whereas the peaks become less sharp with distance from the nozzle;
4) cylindrical or lip waves are 180° out of phase when detected by two microphones placed symmetrically relative to the jet, but Mach waves detected by the symmetrically located microphones do not have a constant phase relationship;
5) the cylindrical waves are weaker than the Mach waves;
6) pressure measurements and accelerometer measurements indicate that the frequency peaks are not correlated with any natural acoustic modes of the shock tube or to nozzle vibration.

5.2.2 High Temperature Analysis

The high temperature data are obtained with a stagnation temperature of 4900°R. The statistically averaged results indicate:

1) cylindrical waves tend to exhibit more than one peak frequency: 3.0 KHz and 5.5 KHz for the underexpanded, 3.3 KHz and 5.0 KHz for the perfectly expanded, and 6.45 KHz for the overexpanded conditions;
2) the higher frequency peaks of the cylindrical waves are roughly 180° out of phase, but the lower frequency peaks appear to be

in phase when detected by the two symmetrically located microphones;

3) the peaks of the Mach waves are higher than the peaks of the cylindrical waves: 10.5 KHz for the underexpanded, 10.0 KHz for the perfectly expanded, and 7.03 KHz for the overexpanded jet;

4) the structure of the cross correlation of the signals from the two symmetrically located microphones in the region of the Mach waves is completely lost in the case of the perfectly expanded jet.

Although there is some positive indication coupling the Mach waves to the lip waves in the low temperature condition, such indication is not evident in the high temperature condition. The observation that the higher frequency peaks of the cylindrical waves are roughly 180° out of phase when detected by the two symmetrically located microphones in the lip wave region for both the low and high temperature jet conditions, indicates that the lip waves are generated by the same mechanism.

5.3 Overall Power Level -- Rectangular Jet

The experimental correlation of the acoustic power or sound power level (PWL) as a function of the jet density ratio for the rectangular jet is plotted in Fig. 15. Because of the non-symmetry of the rectangular nozzle, the calculation of the PWL is performed on a cylindrical surface of radius 30 inches running coaxial to the jet and extending as far as 52 inches downstream from the nozzle exit. The sound

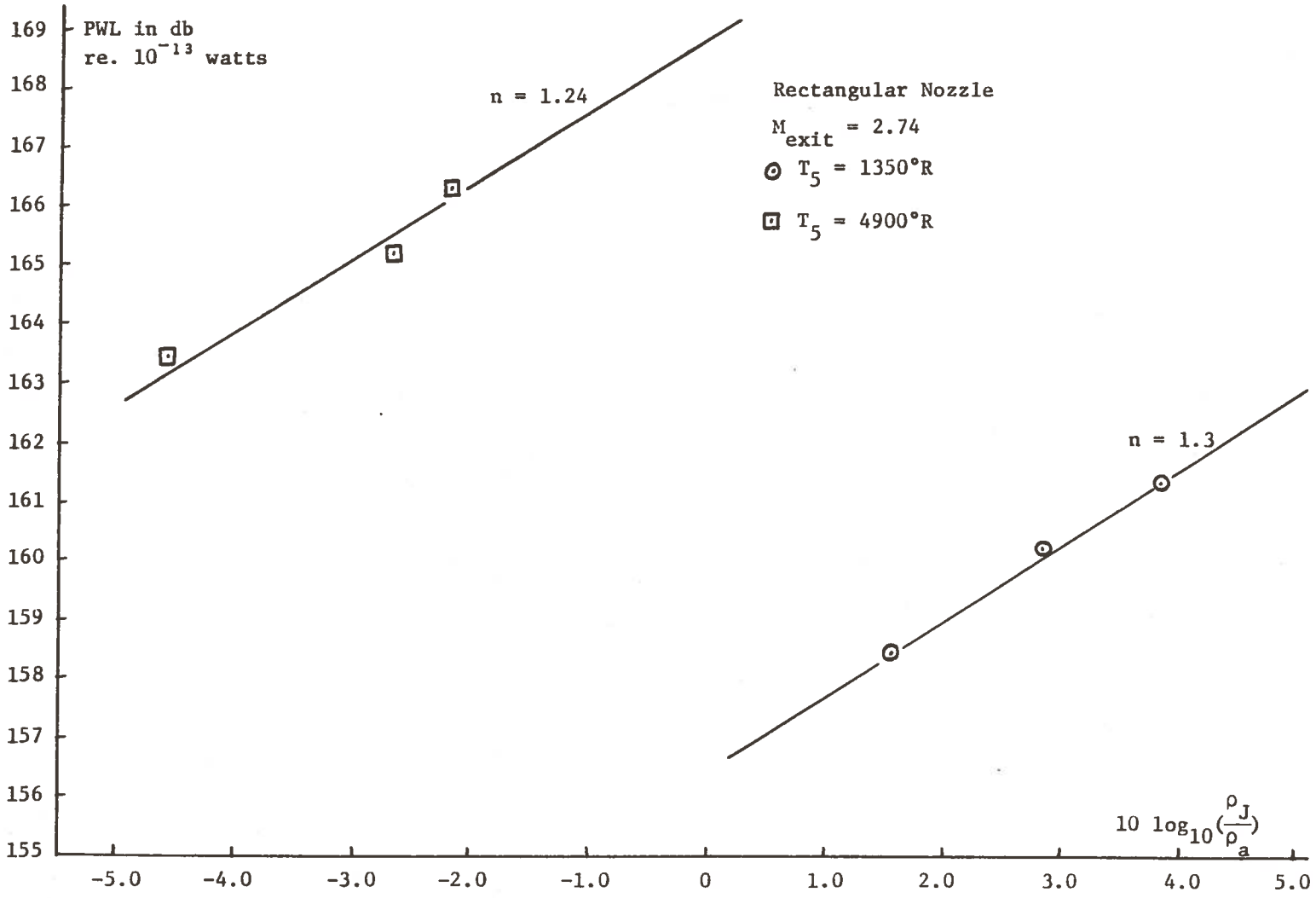

Figure 15: Correction of PWL as a Function of Jet Density Ratio (Rectangular Jet).

pressure level (SPL) on the cylindrical surface is assumed to be elliptical and the average SPL ($\underset{\sim}{P}_n^2$) is given by

$$\underset{\sim}{P}_n^2 = \frac{1}{2\pi} \int_0^{2\pi} \frac{P_1^2 \, P_2^2}{P_2^2 \sin^2\phi + P_1^2 \cos^2\phi} \, d\phi \qquad (5\text{-}3\text{-}1)$$

where P_1^2 and P_2^2 are the SPL along the long and short axes.

The total acoustic power is

$$PWL = \frac{1}{\rho_o c_a} \int_0^L \underset{\sim}{P}_n^2 \, 2\pi R \, dx \qquad (5\text{-}3\text{-}2)$$

The error associated with this method of calculating the acoustic power for the rectangular jet is centered on the assumption of an elliptical SPL distribution on the cylindrical surface and from using Simpson's rule for performing the integration. This error is known as the systematic error and it amounts to ±0.4 decibels. The other source of error is known as the fixed error which is associated with each microphone recording; the fixed errors are the same for both the circular and rectangular nozzles. Hence, only the systematic error is considered when comparing the results of the rectangular and the identical circular nozzle (M_J = 2.74).

The density of the jet is calculated using the equation of state as given in equation (1-5-4). The motivation for using the jet density ratio

as a scaling parameter rather than the stagnation pressure ratio $\frac{P_o}{P_{o\ perf.}}$ as defined in section (1.5) is that both parameters are identical when the jet Mach number and stagnation temperatures are held constant. From equation (1-5-6)

$$\frac{P_o}{P_{o\ perf.}} \propto \left(\frac{\rho_J}{\rho_a}\right) \cdot \frac{1}{M_J^2} \left(\frac{u_J}{C_a}\right)^2 \qquad (5\text{-}3\text{-}3)$$

For a given nozzle and stagnation temperature, M_J and U_J are constant and by varying the stagnation pressure of the jet (corresponding to the overexpanded, perfectly expanded and underexpanded conditions) the density ratio is varied accordingly. As has been discussed in section (1.6) and (1.7), the jet density ratio can be regarded as the Reynolds number based on the viscosity of the jet as from equation (1-7-2)

$$Re_{D_J} \propto \left(\frac{\rho_J}{\rho_a}\right) \qquad (5\text{-}3\text{-}4)$$

From this analysis, the density ratio $\frac{\rho_J}{\rho_a}$ is a good parameter to be used in the scaling law to indicate the dominance of the shock-shear layer or turbulence interaction especially in the circular jet.

From the results given in Fig. 15, the scaling factor for the jet density ratio for the high stagnation temperature condition T_5 = 4900°R is approximately 1.24 whereas for the low stagnation temperature condition T_5 = 1350°R the scaling factor is roughly 1.3.

For a given temperature condition, the acoustic power results indicated in Fig. 15 correspond to the acoustic powers generated by the overexpanded, perfectly expanded and underexpanded rectangular jet. Since the jets are operated in the range of pressures not far from the perfectly expanded pressure condition even for the underexpanded and overexpanded cases, it is not clear whether the present results are valid for the far-overexpanded or far-underexpanded supersonic jets. In the far-overexpanded jet, separation may occur inside the nozzle and the jet may become non-axisymmetric. However, the results should be valid for the range of stagnation pressure ratios $(\frac{P_o}{P_{o\ perf}})$ from $\frac{29}{23}$ to $\frac{14}{23}$ that has been investigated in the experiment.

The value of the scaling factor for the jet density ratio (n_1) as obtained in the experiment is represented by the slope of the line which best fits the experimental data given by the three expansion conditions for a given stagnation jet temperature; as such the value of the scaling factor obtained is only an approximate value. This indicates that the scaling factor for the jet density ratio (n_1) is mainly a function of the jet Mach number and to a lesser extent a function of the jet stagnation temperature. The value of 1.3 is taken as the approximate average value of n_1 for the rectangular jet ($M_J = 2.74$).

In the identical circular jet ($M_J = 2.74$), this scaling factor n_1 is obtained experimentally as 0.6. This apparent discrepancy between the scaling factor for the jet density ratio of the identical circular jet suggests that different noise generating mechanism may be the most important in different nozzle configurations. The scaling factor for the jet density ratio for the two nozzles (rectangular and the identical

circular nozzle) would be roughly the same if the most important noise generating mechanism is the same. In the case of the rectangular nozzle, the jet undergoes a rapid deceleration through a system of strong shocks and the length of the system of shocks is very much shorter than that in the identical circular jet. Based on this observation, the noise generation from shock-turbulence interaction would be rather more important in the circular jet than in the identical rectangular jet. Furthermore, as far as the acoustic near field is concerned the strength of the Mach wave radiation in the rectangular jet is constant along the direction of propagation of the waves because the waves are propagating normal to the long and short axes and form parallel rays. In the circular jet, the Mach waves are diverging forming a source-like flow field and the strength of the waves falls off like the reciprocal of the distance from the jet axis. It must be cautioned that in the acoustic far field the strength of the Mach waves for both the rectangular and circular jets falls off like the reciprocal of the radial distance.

From this analysis, an observation can be drawn: that Mach wave radiation is more important in the rectangular jet than in the circular jet where shock-turbulence interaction is much more important.

Shadowgraphs of the rectangular jet, as given in Ref. 8, indicate that practically no spherical acoustic waves are seen to radiate from the shock tips; whereas in the shadowgraphs of the identical circular jet, as given in Ref. 2, the spherical acoustic waves are very prominent. This further suggests that Mach wave radiation is likely to be more important in the rectangular jet than in the circular jet.

The total acoustic power for $\frac{\rho_J}{\rho_a} = 1.0$ is obtained by extrapolating from the experimental correlation of the total acoustic power as the

function of the jet density ratio, as given in Fig. 15. The motivation for the extrapolation is to obtain the total acoustic power for $\frac{\rho_J}{\rho_a} = 1.0$ as a function of the jet stagnation temperature $\frac{T_o}{T_{o\ perf}}$, as defined in section (1.8). For convenience, the jet velocity ratio $\frac{U_J}{C_a}$ is chosen as the second scaling parameter rather than the jet stagnation temperature $\frac{T_o}{T_{o\ perf}}$ since the two parameters are equivalent for a given jet Mach number (M_J).

From equation (1-8-3)

$$\frac{T_o}{T_{o\ perf}} \propto \left(\frac{U_J}{C_a}\right)^2 \qquad (5\text{-}3\text{-}5)$$

The acoustic power correlation for $\frac{\rho_J}{\rho_a} = 1.0$ as a function of the jet ratio $\frac{U_J}{C_a}$ is given in Fig. 16. Since in the rectangular jet, data for only 2 stagnation temperature conditions are available, it is not clear as to how the scaling factor of the jet velocity ratio varies as the function of the jet Mach number M_J and the velocity ratio $\frac{C_J}{C_a}$.

The scaling factor of the jet velocity ratio, n_2, is expected to vary not only as a function of the jet Mach number M_J but also as a function of the velocity ratio $\frac{C_J}{C_a}$; that is to say, the scaling factor n_2 for the jet velocity ratio is going to vary as a function of the Eddy Convective Mach Number, M_c, itself. But since M_c is approximately

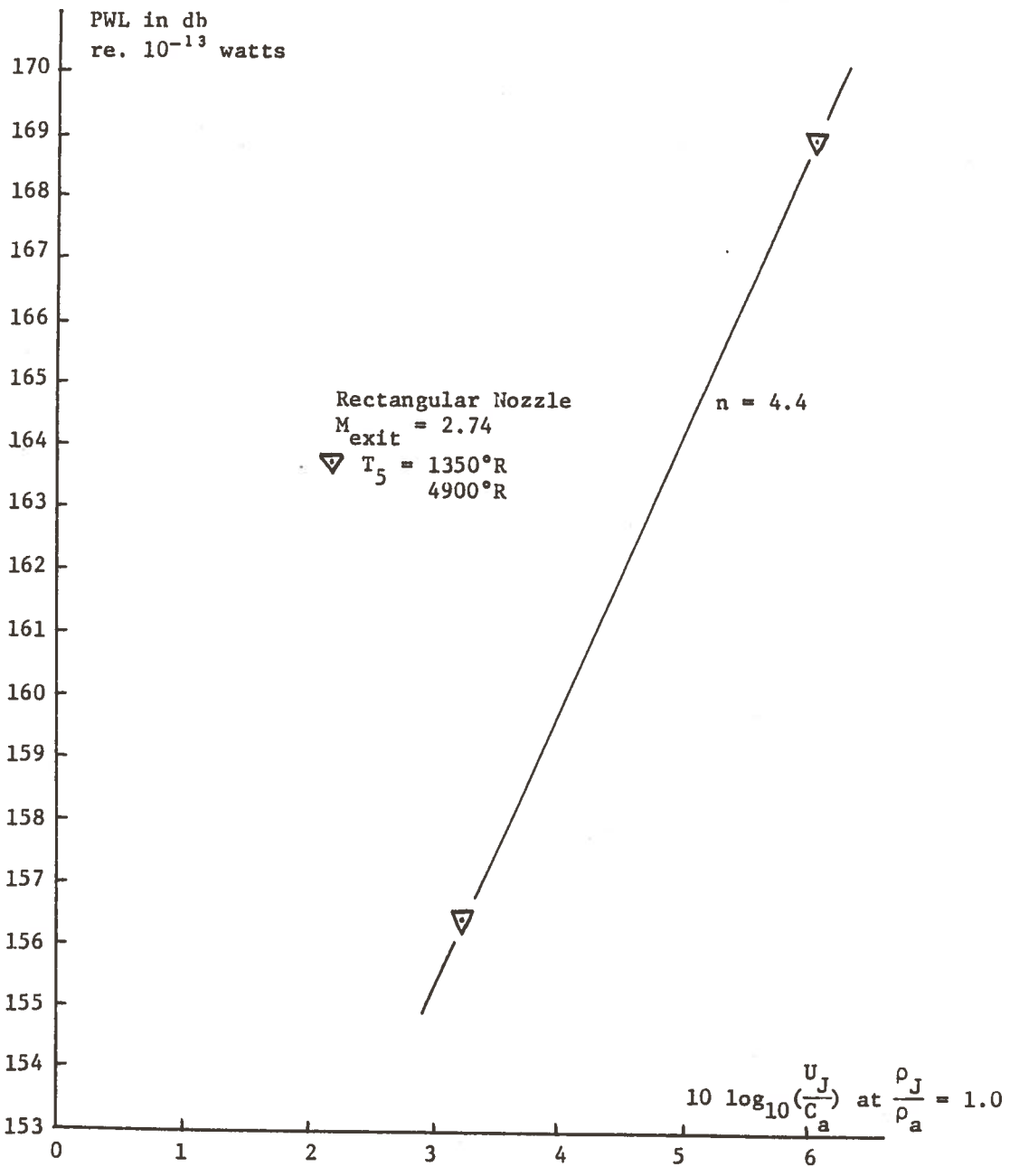

Figure 16: Correlation of PWL at $\frac{\rho_J}{\rho_a} = 1$ as a Function of Jet Velocity Ratio $\frac{U_J}{C_a}$ (Rectangular Jet).

0.5 $(\frac{U_J}{C_a})$ to 0.7 $(\frac{U_J}{C_a})$, the scaling factor n_2 is going to vary as a function of the jet velocity ratio $\frac{U_J}{C_a}$, and this analysis seems consistent with the observation that the total acoustic power varies as the eight-power of the jet velocity ratio in the subsonic jet and the third-power of the jet velocity ratio in the hypersonic jets.

Based on limited data that is available for the rectangular jet (M_J = 2.74) the value of the scaling factor is roughly 4.4, and the total acoustic power generated by the rectangular jet (M_J = 2.74) can be given by the empirical relation

$$PWL = 142.25 + 10\log_{10}\left(\frac{U_J}{C_a}\right)^{4.4} + 9.3\ 10\log_{10}\left(\frac{\rho_J}{\rho_a}\right)^{1.3} \qquad (5\text{-}3\text{-}6)$$

where PWL is given in decibels reference at 10^{-13} watts.

The relation given above for the total acoustic power generated by the rectangular jet (M_J = 2.74) is only preliminary and should be verified with additional data.

5.4 Acoustic Power from Eddy Mach Wave Radiation

The results on Mach wave radiation indicate that the acoustic power generated by means of Mach wave radiation is proportional to the jet density ratio $\frac{\rho_J}{\rho_a}$ to the power $(2\phi_1 + 0.35)$, and to the jet velocity ratio $\frac{U_J}{C_a}$ to the power $(8 - 5\phi_2 - 0.70)$. This means that <u>if</u> eddy Mach wave radiation is indeed the most important noise generating mechanism in the rectangular jet, as suggested by the present analysis, the average power of 1.3 for the jet density ratio dependence (rectangular jet) corresponds

to the factor $(2\phi_1 + 0.35)$ as derived from the eddy Mach wave radiation theory. This implies that

$$\phi_1 \simeq 0.48$$

$$\phi_2 \simeq 0.58 \qquad \text{for } M_J = 2.74$$

-- very reasonable values for these exponents.

The values of the scaling factors n_1 and n_2 obtained are only approximate values and so the values of ϕ_1 and ϕ_2 are also approximate values; additional data have to be taken before the variation of ϕ_1 and ϕ_2 with jet velocity ratio and jet Mach numbers is known.

5.5 Overall Power Level of Circular Jets

The correlations of the acoustic power with jet density ratio $\frac{\rho_J}{\rho_a}$ for the circular jets $M_J = 2.74$, 2.3 and 1.8 are shown in Figs. 17, 18 and 19. The scaling factor (n_1) for the jet density ratio shows a strong dependence on the jet Mach number only, although it does exhibit a weak dependence on the stagnation temperature of the jet. For the circular jets $(M_J = 2.74)$ the scaling factor of the jet density ratio varies between 0.55 to 0.65 for the six stagnation temperatures investigated, as indicated in Fig. 17. An average value of 0.6 is taken for the scaling factor n_1 in this case.

For the other two circular jets $(M_J = 2.3)$ and $(M_J = 1.8)$ the average scaling factors of the jet density ratio are 0.8 and 1.5 respectively. The results suggest that at high supersonic jet Mach numbers, the value of n_1 is going to level off to zero. At low supersonic jet Mach numbers,

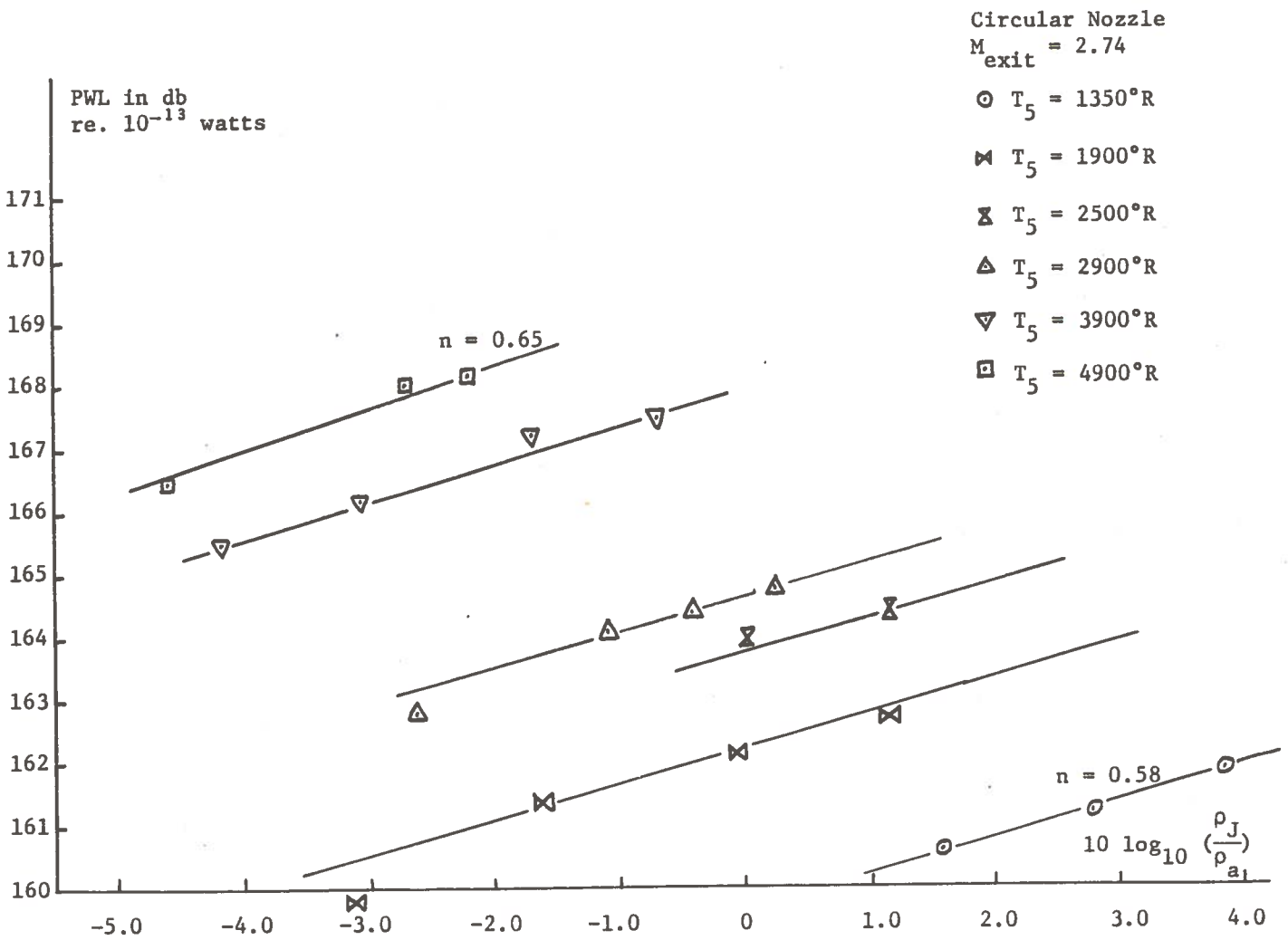

Figure 17: Correlation of PWL as a Function of Jet Density Ratio (Circular Jet, M_J = 2.74).

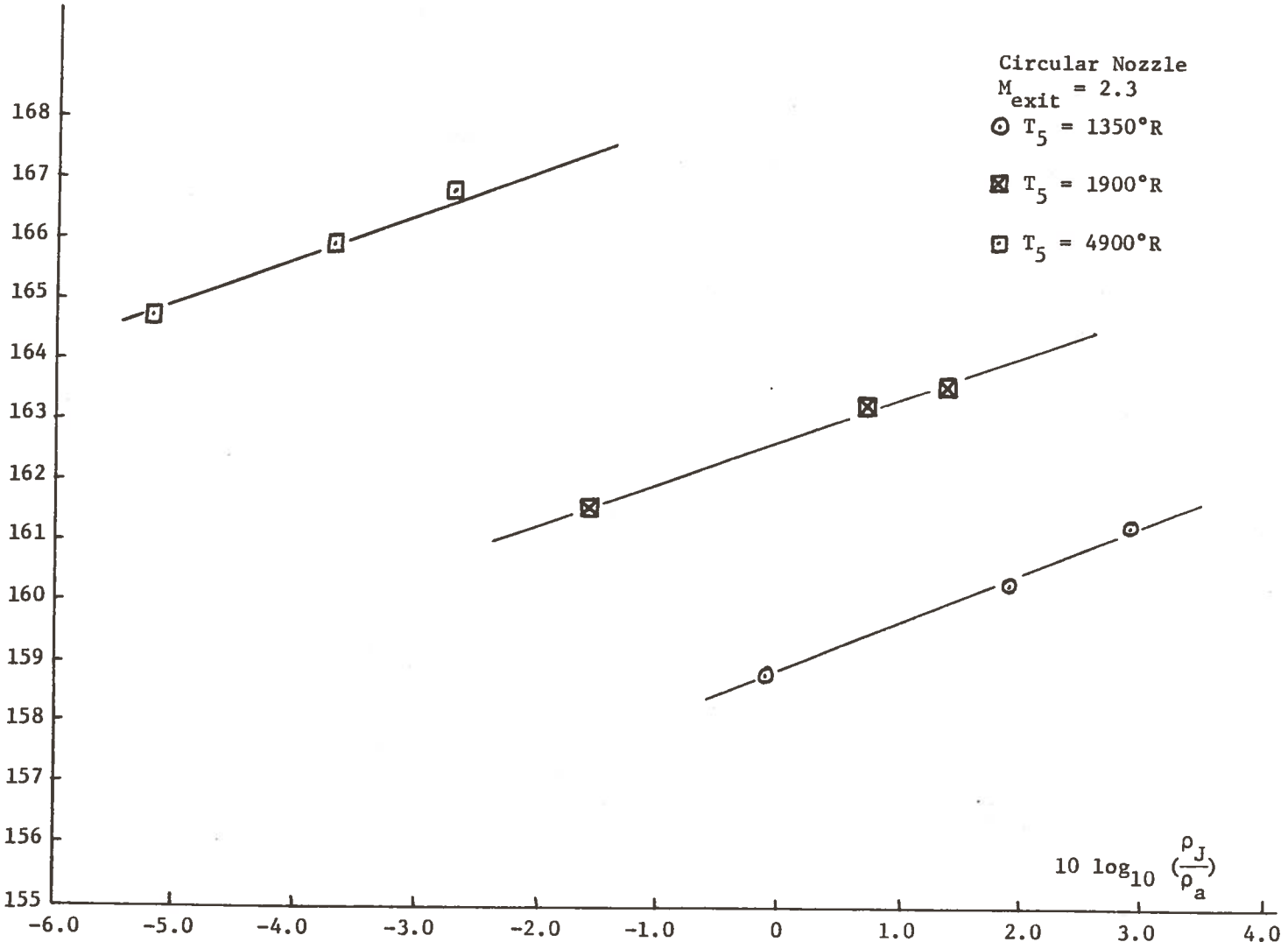

Figure 18: Correlation of PWL as a Function of Jet Density Ratio (Circular Jet, M_J = 2.3)

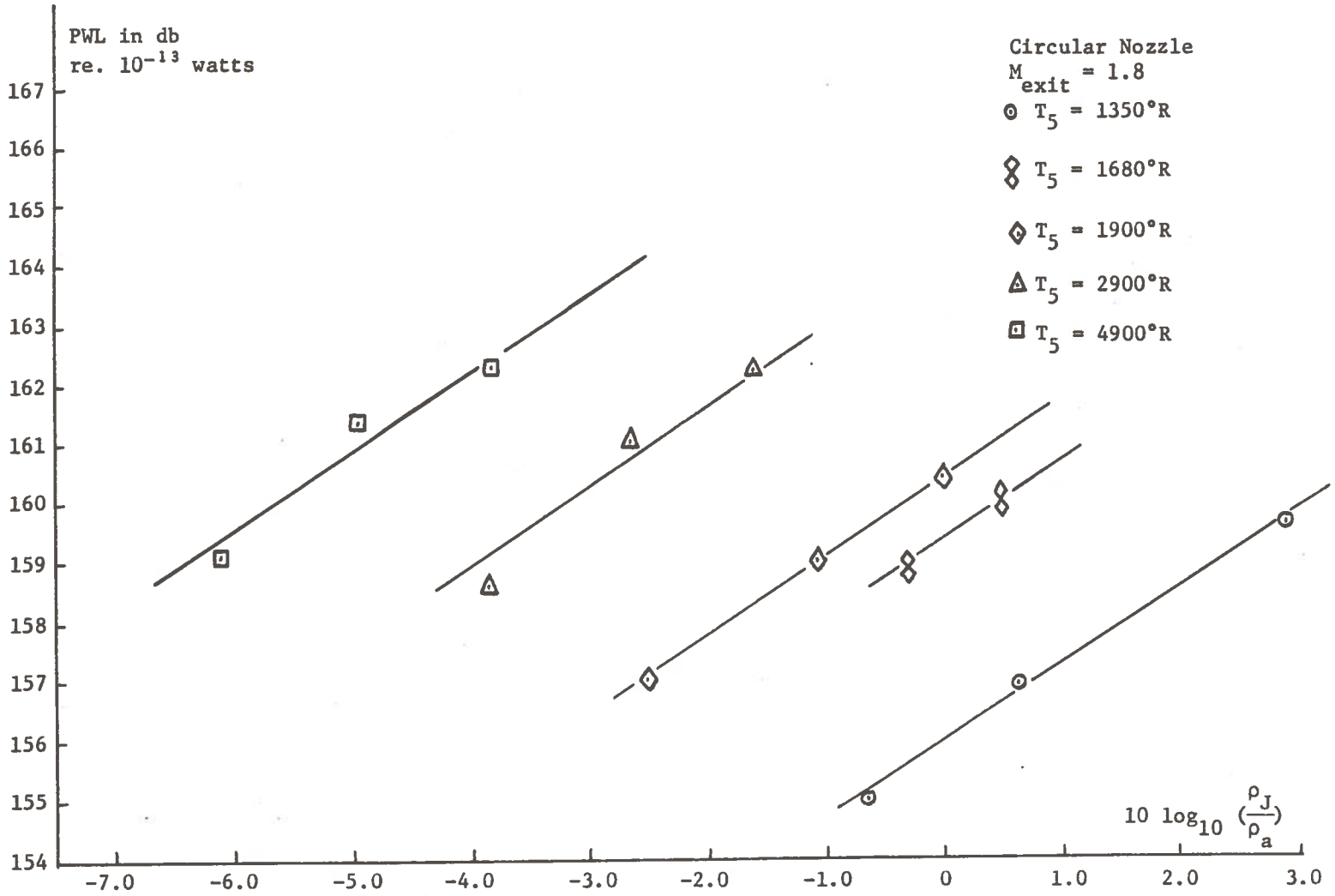

Figure 19: Correlation of PWL as a Function of Jet Density Ratio (Circular Jet, M_J = 1.8).

this scaling factor of the jet density ratio is going to approach the value of 2.

For the range of the jet Mach numbers (M_J = 1.8 to M_J = 2.74) investigated in this experiment, the value of the scaling factor n_1 for the jet density ratio can be approximated by the relation

$$n_1 = 3.25 - \frac{14.8}{M_J} + \frac{21}{M_J^2} \qquad (5\text{-}5\text{-}1)$$

where n_1 is the value of the scaling factor for the jet density ratio. Outside the range of jet Mach numbers (M_J = 1.8) to (M_J = 2.74) the above empirical expression for n_1 may not be valid. Additional data must be taken for jet Mach numbers near one and for jet Mach numbers greater than one before a complete relation for n_1 can be obtained.

The total acoustic power for $\frac{\rho_J}{\rho_a}$ = 1.0 for the three circular jets as a function of the jet velocity ratio $\frac{U_J}{C_a}$ is given in Fig. 20.

The scaling factor n_2 of the jet velocity ratio given by the slopes of the curves in Fig. 20 is mainly a function of the jet velocity ratio $\frac{U_J}{C_a}$ and the jet Mach number M_J. For the M_J = 1.8 circular jet, the values of the scaling factor n_2 vary from 7.0 at low jet velocity ratio to approximately 3.0 at higher jet velocity ratio. The values of the scaling factor n_2 vary from 5.0 to 3.0 for the M_J = 2.3 circular jet and from 3.5 to 3.0 for the M_J = 2.74 circular jet.

For the range of jet velocity ratio ($2.5 \leq \frac{U_J}{C_a} \leq 6.05$), as investigated in the experiment, the values of the scaling factor n_2 for the jet velocity ratio can be represented empirically as

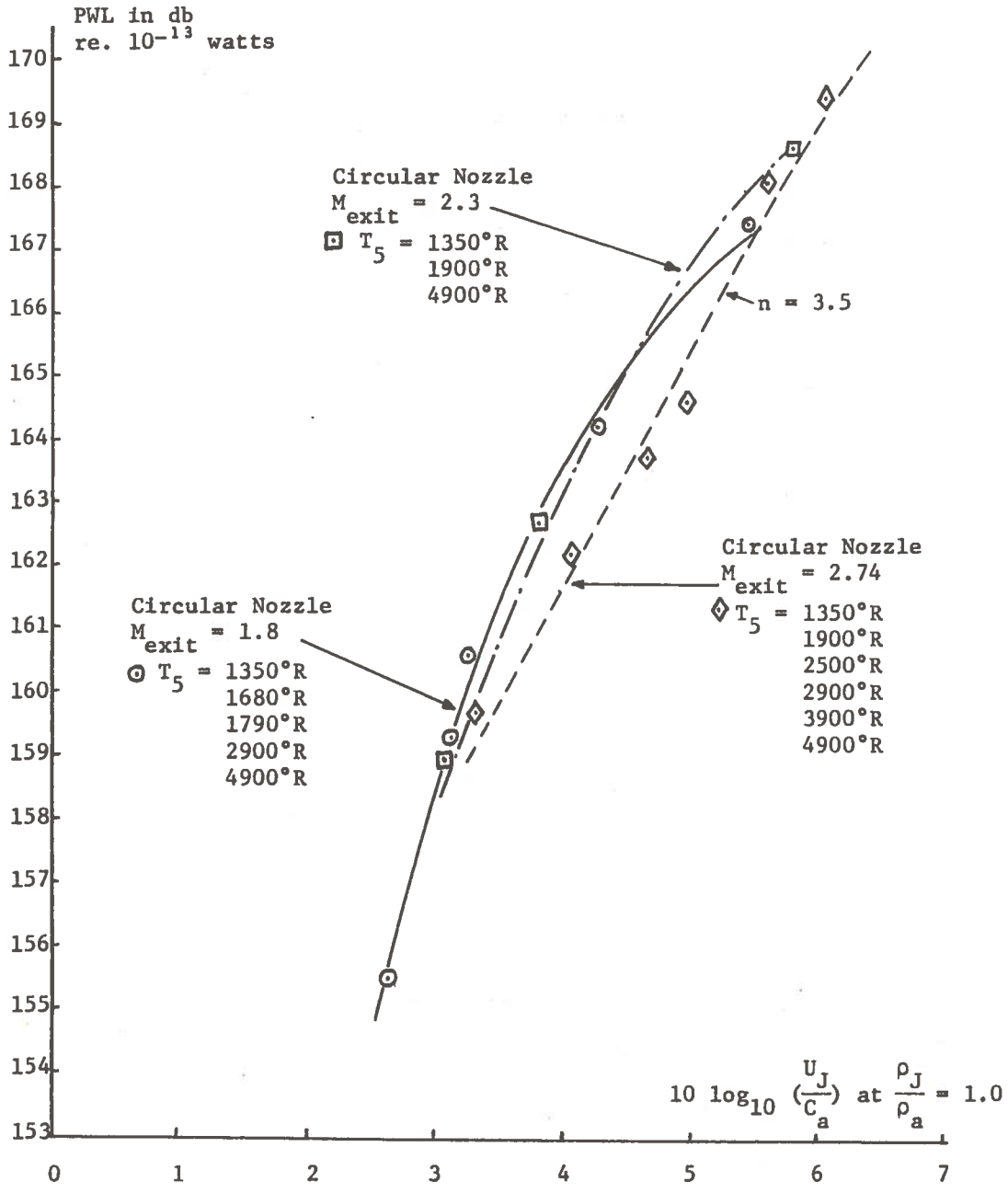

Figure 20: Correlation of PWL (at $\frac{\rho_J}{\rho_a} = 1.0$) as a Function of Jet Velocity Ratio.
(Circular Jets, M_J = 2.74, 2.3, and 1.8).

$$n_2 = 5.2 - \frac{26.2}{\left[10 \log_{10}\left(\frac{u_J}{C_a}\right)\right]} + \frac{77}{\left[10 \log_{10}\left(\frac{u_J}{C_a}\right)\right]^2} \qquad (5\text{-}5\text{-}2)$$

The empirical relation or curve which gives the best fit to all the data for the three circular nozzles is obtained as

$$PWL = 143.8 + 10 \log_{10}\left(\frac{\rho_J}{\rho_a}\right)^{n_1} + 10\,C \log_{10}\left(\frac{u_J}{C_a}\right)^{n_2} \qquad (5\text{-}5\text{-}3)$$

where

$$n_1 = 3.25 - \frac{14.8}{M_J} + \frac{21}{M_J^2}$$

$$n_2 = 5.2 - \frac{26.2}{\left[10 \log_{10}\left(\frac{u_J}{C_a}\right)\right]} + \frac{77}{\left[10 \log_{10}\left(\frac{u_J}{C_a}\right)\right]^2}$$

and C is a function of the jet velocity ratio $\frac{U_J}{C_a}$, and PWL is expressed in decibel reference at 10^{-13} watts.

The values of C as a function of $10 \log_{10} (\frac{U_J}{C_a})$ are given here:

$10 \log_{10} (\frac{U_J}{C_a})$	C
2.5	0.6
3.0	1.0
3.5	1.23
4.0	1.33
4.5	1.43
5.0	1.43
5.5	1.43

Expression (5-5-3) is derived using data taken in this experiment and since there is some scatter of the data, the above empirical expression for the total acoustic power level generated by a circular jet gives an accuracy within ± 1 decibel. Furthermore, it is important to note that the above expression for the total acoustic power is valid for the range of jet Mach numbers from 1.8 to 2.74 and jet velocity ratio of 2.5 to 6.0. Beyond these ranges of jet Mach number and jet velocity ratio, additional data are needed.

5.6 Acoustic Power from Shock-Turbulence Interaction

Based on the model that shock-turbulence interaction is the most important noise generating mechanism in the circular supersonic jet, the scaling factors, n_1 and n_2, of the acoustic power from the circular jet should correspond to the scaling factors derived from the theory of shock-turbulence interaction.

From the analysis of the shock-turbulence interaction, the scaling law of the acoustic power is in the form of

$$PWL \propto \left(\frac{\rho_J}{\rho_a}\right)^{0.5 + 0.35a} \left(\frac{u_J}{C_a}\right)^{3.0 + 0.7a} \qquad (5\text{-}6\text{-}1)$$

This means that the factor (0.5 + 0.35a) corresponds to the relation for n_1, the scaling factor of the jet density ratio:

$$0.5 + 0.35a = 3.25 + \frac{14.8}{M_J} + \frac{21}{M_J^2} \qquad (5\text{-}6\text{-}2)$$

$$0.35a = 2.75 - \frac{14.8}{M_J} + \frac{21}{M_J^2}$$

and so the scaling factor for the jet velocity ratio, as predicted by the shock-turbulence interaction analysis is

$$(3.0 + 0.7a) = 8.5 - \frac{29.6}{M_J} + \frac{42}{M_J^2} \qquad (5\text{-}6\text{-}3)$$

It is clear that, based on the model of shock-turbulence interaction as the main noise generating mechanism in the circular jet, the scaling factor given by equation (5-5-3) is expressed only as a function of the jet Mach number M_J, whereas from the experimental results and the empirical correlation derived in expression (5-5-2) the scaling factor n_2 for the jet velocity ratio varies both as a function of M_J and C_J.

M_J	Scaling Factor for $\frac{U_J}{C_a}$ Predicted from the Theory of Shock-Turbulence Interaction	n_2 Experimental results [Slope of PWL vs 10 $\log_{10}$ $(\frac{U_J}{C_a})$]
2.74	2.9	3.5 to 3.0
2.30	3.5	5.0 to 3.0
1.80	5.1	7.0 to 3.0

The predicted value for the scaling factor n_2 of the jet velocity ratio based on the theory of the shock-turbulence interaction seems to give a somewhat average value for the slope of the curve of PWL vs 10 $\log_{10}$ $(\frac{U_J}{C_a})$.

The only limitation in the present model of shock-turbulence interaction as the main noise generating mechanism in the circular jet is that it does not predict the changing of the slopes of the curve of the PWL vs 10 $\log_{10}$ $(\frac{U_J}{C_a})$.

VI. CONCLUSIONS

Although the work described above cannot be considered complete because of the complexity of the subject, some conclusions can be reached:

1) The shock tunnel is a flexible and practical tool for the study of supersonic jet noise. It provides a quasi-steady jet, but for a limited time (10 msec); however, this limitation can be largely overcome by fast data gathering and processing. The short operation time provides a natural anechoic test environment.

2) The comparison of a rectangular nozzle with a circular nozzle of identical flow characteristics provides a good means for the discrimination of the relative importance of jet noise mechanisms. Noise mechanisms induced at the surface of the jet are therefore found to be dominant in the rectangular jet, whereas volume phenomena such as shock induced noise are more important in the axisymmetric jet. The ellipticity of the directivity pattern for the rectangular jet was previously reported.

3) Measured sound directivity and Mach waves propagation direction obtained from shadowgraphs indicate that Mach waves contribute importantly to the noise produced by a rectangular jet. The experimental scaling law for the rectangular jet is given, and it can be interpreted in terms of the theoretical scaling law for Mach wave radiation derived in the text.

4) Measured sound directivity, interpretation of shadowgraphs and scaling of noise indicate stronger influence of shock-induced noise. The experimental scaling law determined for the circular jet cannot be completely interpreted in terms of the theoretical scaling law derived in the text for shock-turbulence interaction.

5) The quasi two-dimensional flow from the rectangular nozzle gave an opportunity to study Mach and nozzle lip waves for both low and high temperature jets. Statistical observations made on an ensemble of runs indicate that lip waves have well-defined frequency peaks and that waves emanating from opposite lips are out of phase. Mach waves in opposing sides of the jet do not appear to have a constant phase relationship.

At low temperature, with jet and ambient air densities nearly equal, lip waves frequencies are found in the Mach wave spectrum, indicating the propagation of lip-originated disturbances along the shear layer. At high temperature, with jet density much smaller than ambient, Mach waves spectrum has no relation to lip waves spectrum, and shear layer instabilities dominate the Mach waves field.

APPENDIX A

SCALING LAW FOR TOTAL ACOUSTIC POWER OF AN AIR JET

For the case of air jets ($\gamma = 1.4$), Powell[22] suggested that the spacing of the shock cell is given by

$$\frac{s}{d} = 1.2 \left(R^* - R_c\right)^{0.5} \tag{A-1}$$

where R^* = pressure ratio = $\frac{P_o}{P_a}$

R_c = critical pressure ratio for air

s = shock separation

d = nozzle diameter.

Therefore, the form of the scaling law for the total acoustic power of an air jet due to the mechanism of eddy Mach wave generation is

$$PWL_{eddy} = \text{Constant} \times F(M_J) \left(\frac{\rho_J}{\rho_a}\right)^{2\phi_1 + 0.5} \left(\frac{u_J}{C_a}\right)^{9 - 5\phi_2} \tag{A-2}$$

Similarly, the form of the scaling law for the total acoustic power of an air jet due to the mechanism of shock-turbulence interaction is

$$PWL_{\substack{\text{shock-turb.} \\ \text{interaction}}} = \text{Constant} \times G(M_J) \left(\frac{\rho_J}{\rho_a}\right)^{0.5 + 0.5a} \left(\frac{u_J}{C_a}\right)^{3.0 + a} \tag{A-3}$$

APPENDIX B

CALCULATION OF STRENGTHS OF FIRST FOUR SHOCKS IN OVEREXPANDED AND UNDEREXPANDED JET, $M_J = 2.74$

The strength of the first four shocks in the supersonic region of the jet is calculated for the overexpanded $\frac{P_J}{P_a} = \frac{17}{23}$ and the underexpanded $\frac{P_J}{P_a} = \frac{29}{23}$ jets for the case of jet Mach number 2.74, as shown in Fig. 21.

Overexpanded Jet

$$\frac{P_J}{P_a} = \frac{17}{23} \ , \ M_J = 2.74 \ , \ \gamma = 1.67$$

1st shock:

$M_{n1} = 1.118$

$\beta_1 = 24°5'$

$\theta_1 = 3°16'$

2nd shock:

$M_{n2} = 1.094$

$\frac{P_a}{P_3} = 0.754$

$\beta_2 = 22°20'$

$\theta_2 = 3°16'$

3rd shock:

$M_{n3} = 1.084$

$\beta_5 = 23°23'$

$\theta_3 = 2°23'$

$\frac{P_5}{P_a} = 0.781$

4th shock:

$M_{n4} = 1.079$

$\beta_6 = 22°20'$

$\theta_4 = 2°23'$

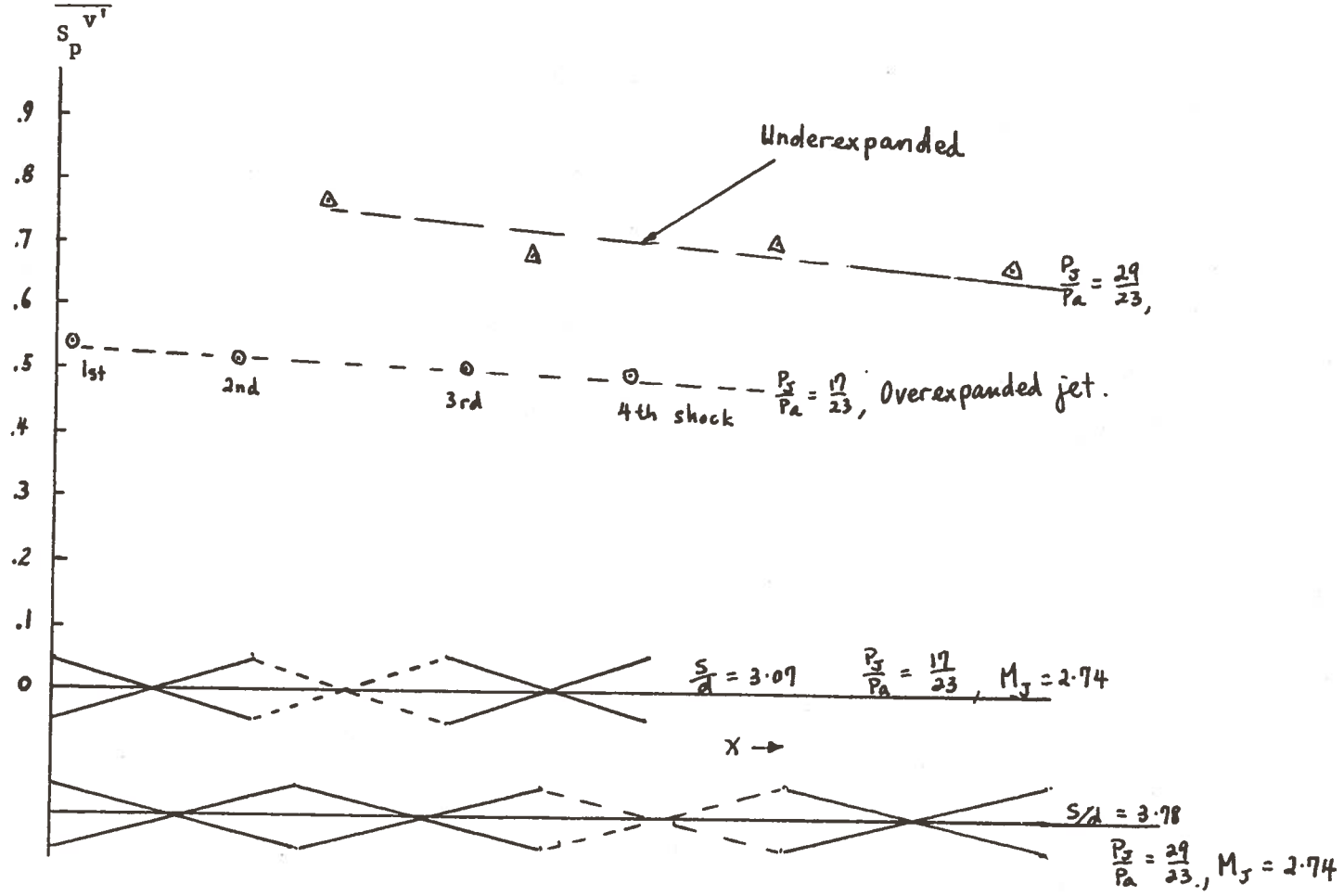

Figure 21: Values of the Average Transfer Functions $\overline{S_p}^{v'}$ for the 1st, 2nd, 3rd and 4th Shocks.

Underexpanded Jet

$$\frac{P_J}{P_a} = \frac{29}{23} \text{ , } M_J = 2.74$$

1st shock:

$M_{n1} = 1.219$

$\beta_1 = 23°5'$

$\theta_1 = 5°15'$

$\frac{P_3}{P_a} = \frac{23}{37.0}$

2nd shock:

$M_{n2} = 1.15$

$\beta_2 = 19°42'$

$\theta_1 = 5°15'$

$\frac{P_a}{P_4} = 0.596$

3rd shock:

$M_{n3} = 1.156$

$\beta_5 = 20°30'$

$\theta_3 = 3°16'$

$\frac{P_5}{P_a} = 0.58$

4th shock:

$M_{n4} = 1.128$

$\beta_6 = 19°14'$

$\theta_4 = 3°16'$

APPENDIX C

REPORT OF INVENTIONS APPENDIX

Investigation of the work performed under this contract indicates that no inventions, discoveries, improvements or innovations, reportable within the meaning of the contract's patent clause, have resulted.

REFERENCES

1. Lighthill, M. J., "On Sound Generated Aerodynamically"; I. General Theory, Proc. of Roy. Soc., Ser. A, 211, 1952; II. Turbulence as a Source of Sound, Proc. of Roy. Soc., Ser. A, 222, 1954.

2. Louis, J. F., Letty, R. M. and Patel, J. R., "A Systematic Study of Supersonic Jet Noise", GTL Report No. 106, M.I.T., 1971.

3. Kerrebrock, J. L., "The Interaction of Flow Discontinuities with Small Disturbances in a Compressible Fluid", Ph.D. Thesis, Cal. Inst. of Tech., 1956.

4. Tam, C. K. W., "Directional Acoustic Radiation from a Supersonic Jet Generated by Shear Layer Instability", J. of Fluid Mech., 46, 1971, p. 757.

5. Nagamatsu, H. T. and Horvay, G., "Supersonic Jet Noise", AIAA Paper No. 70-237, 1970.

6. Lighthill, M. J., "Jet Noise", AIAA J., 1, 1963, pp. 1507-17.

7. Ribner, H. S., "Strength Distribution of Noise Sources along a Jet", J. of Acoustical Soc. of Amer., 30, 1958, p. 876.

8. Patel, J. R., "Jet Noise from a Supersonic Rectangular Nozzle", S.M. Thesis, Dept. of Aero. and Astro., M.I.T., 1971.

9. Coles, G. M., "The Noise of High Velocity Jets", Rolls Royce (Derby), Brochure A. P. 11, 1961.

10. Coles, G. M., "The Noise of High Velocity Jets", Rolls Royce (Derby), unpublished report, 1961.

11. Lassiter, L. W. and Hubbard, H. H., "Experimental Studies of Noise from Subsonic Jets in Still Air", NACA TN 2757, 1952.

12. Ffowcs Williams, J. E., "Noise from Turbulence Convected at High Speed", Phil. Trans. Roy. Soc., A255, 1963, pp. 469-503.

13. Price, R. H., "Measurements of the Time-Averaged Density Structure and Spatial Distributions of Fluctuations in a Supersonic Argon Jet", S.B. Thesis, Dept. of Physics, M.I.T., 1971.

14. Nagamatsu, H. T., Sheer, R. E. and Gill, M. S., "Flow and Acoustic Characteristics of Subsonic and Supersonic Jets from Convergent Nozzle", AIAA Paper No. 70-802, 1970.

15. Liepman, H. W. and A. Roshko, Elements of Gasdynamics, John Wiley & Sons, Inc., New York, 1963.

16. Goldberg, P., "Upstream History and Apparent Stress in Turbulent Boundary Layers", GTL Report No. 85, M.I.T., 1966.

17. Louis, J. F., Letty, R. P. and Patel, J. R., "A Systematic Study of Supersonic Jet Noise", AIAA Paper No. 72-641, 1972.

18. Woodley, J. G., "Performance Estimates for a Reflected Shock Tunnel with a Modified Driver to Produce High Test-Section Reynolds Numbers", (R.A.E. Farnborough) NTIS Paper No. ARC-CP-1057, 1969.

19. Probst, C., "Instruction Manual for the GTL A/D Transmission and A/D Conversion", Gas Turbine Laboratory, M.I.T., 1972, unpub.

20. Simcox, C. D., "Effect of Temperature and Shock Structure on Choked Jet Noise Characteristics", AIAA Paper No. 71-582, 1971.

21. Letty, R. P., "Study of Jet Noise from a Supersonic Axisymmetric Nozzle", S.M. Thesis, Dept. of Aero. and Astro., M.I.T., 1971.